Alzheimer's brain inoculation in Aß-plaque bearing mice: synaptic loss is linked to tau seeding and low microglial activity

Suzanne Lam[1,2], Susana Boluda[3,4], Anne-Sophie Hérard[1,2], Fanny Petit[1,2], Sabiha Eddarkaoui[5], Karine Cambon[1,2], The Brainbank Neuro-CEB Neuropathology Network[4,§], Jean-Luc Picq[1,2,6], Luc Buée[5], Charles Duyckaerts[3,4], Stéphane Haïk[3,4], Marc Dhenain[1,2]

[1] Université Paris-Saclay, CEA, CNRS, Laboratoire des Maladies Neurodégénératives, 18 Route du Panorama, F-92265 Fontenay-aux-Roses, France.
[2] Commissariat à l'Energie Atomique et aux Energies Alternatives (CEA), Direction de la Recherche Fondamentale (DRF), Institut François Jacob, MIRCen, 18 Route du Panorama, F-92265 Fontenay-aux-Roses, France
[3] ICM Institut du Cerveau et de la Moelle épinière, CNRS UMR7225, INSERM U1127, Sorbonne Université, Hôpital de la Pitié-Salpêtrière, Paris, France
[4] GIE Neuro-CEB/Neuropathologist Network: Plate-Forme de Ressources Biologiques, Bâtiment Roger Baillet, Hôpital de la Pitié-Salpêtrière, 47-83 boulevard de l'Hôpital, 75651 Paris Cedex 13.
[5] Université de Lille, Inserm, CHU-Lille, Lille Neuroscience & Cognition, Alzheimer & Tauopathies, LabEx DISTALZ, Rue Polonovski, 59045 Lille, France
[6] Laboratoire de Psychopathologie et de Neuropsychologie, EA, 2027, Université Paris 8, St-Denis, France

[§] GIE Neuro-CEB: Charles Duyckaerts, Véronique Sazdovitch, Sabrina Leclère-Turbant, and Marie-Claire Artaud-Botté; The national network includes the following neuropathologists: Anne Vital (Bordeaux), Françoise Chapon (Caen), Jean-Louis Kemeny (Clermont-Ferrand), Claude-Alain Maurage & Vincent Deramecourt (Lille), David Meyronet & Nathalie Streichenberger (Lyon), André Maues de Paula (Marseille), Valérie Rigau (Montpellier), Fanny Vandenbos-Burel (Nice), Charles Duyckaerts (Paris), Danielle Seilhean (Paris), Véronique Sazdovitch (Paris), Serge Milin (Poitiers), Dan Christian Chiforeanu (Rennes), Annie Laquerrière (Rouen), Béatrice Lannes (Strasbourg), Marie-Bernadette Delisle & Emmanuelle Uro-Coste (Toulouse).

Corresponding author

Marc Dhenain, DVM, PhD
Commissariat à l'Energie Atomique et aux Energies Alternatives (CEA), Direction de la Recherche Fondamentale (DRF), Institut François Jacob, MIRCen, 18 Route du Panorama, F-92265 Fontenay-aux-Roses, France
E-mail: marc.dhenain@cea.fr

Acknowlegements

We thank Martine Guillermier for surgical expertise during inoculation of brain extracts to animals. The project was funded by the Association France-Alzheimer. It was performed in a core facility supported by/member of NeurATRIS - ANR-11-INBS-0011. It was also supported by internal funds from the Laboratory of Neurodegenerative Diseases and MIRCen. We thank the donors and the Brain Donation Program of the "The Brainbank Neuro- CEB Neuropathology Network" run by a consortium of Patient Associations: ARSLA (association for research on amyotrophic lateral sclerosis), CSC (cerebellar ataxias), Fondation ARSEP (association for research on multiple sclerosis), France DFT (fronto-temporal dementia), Fondation Vaincre Alzheimer, France Parkinson, with the support of Fondation Plan Alzheimer and IHU A-ICM for providing the brain samples used in this study.

Abstract

Alzheimer's disease (AD) is characterized by synaptic alterations that lead to cognitive impairments and by a number of lesions including extracellular amyloid-β (Aβ) plaques, intracellular tau accumulation and neuroinflammation. The contribution of these lesions to synaptic alterations is still debated. Through the intracerebral injection of human AD brain extracts into an Aβ plaque–bearing mouse model that does not overexpress tau we recapitulated all these AD lesions. In particular neuritic plaques, AD-like neurofibrillary tangles and neuropil threads, that spread through the brain, were identified and characterized. Interestingly neuritic plaques but not other tau-positive lesions were observed in control-inoculated animals as well as in non-inoculated amyloid-bearing mice, suggesting that these lesions do not require exogeneous tau to be initiated. Inoculation of different human AD brain extracts to mice led to lesional heterogeneity and to enhanced synaptic loss and cognitive impairments. Relationships between synaptic alterations or cognitive impairments and AD pathology were evaluated by exploiting the induced lesional heterogeneity. Synaptic loss and cognitive deficits were associated with the severity of tau lesions and to lower microglial load, but not to amyloid load. Our results outline that new mouse models of AD bearing both Aβ plaques and tau lesions, and based on AD brain extracts inoculation, allow to investigate AD neurodegenerative processes. They highlight the contribution of tau to synaptic impairments in a model that does not rely on genetic manipulation of tau protein and indicate that microglial activity may protect against synaptic loss.

Keywords

Alzheimer's disease; microglia; synaptotoxicity; tau; transmission

Introduction

Alzheimer's disease (AD) is a clinical entity leading to cognitive deficits that are strongly correlated with synaptic alterations [32]. AD core lesions include amyloid-β (Aβ) plaques and intracellular tau accumulations that spread in a highly stereotyped pattern through the brain [4]. Tau pathology begins in the entorhinal cortex and hippocampus (Braak stages I to III or IV) in the absence of Aβ deposits (Aβ phase 0). Tau pathology is later found in the isocortex (Braak stages V and VI) together with Aβ deposits (Aβ phase 1 or higher) and cognitive impairments [4, 9]. At these late stages, tau spreading from the medial temporal lobe to cortical amyloid-positive regions is strongly correlated to clinical decline [2, 23]. The respective contribution of AD core lesions to synaptic and cognitive deficits are still partly unknown. Studies in mice and other experimental models suggest that both Aβ [29, 30] and tau [6, 18, 25] can induce synaptic deficits. Microglia is a third key player involved in AD pathophysiology [27]. Indeed, the proliferation and activation of microglia, clustering around amyloid plaques, are prominent features of AD. Several evidence (mostly in mouse models) suggest that increased microglia surrounding amyloid plaques are responsible for neuronal damages. However, human genetic evidence, exemplified by the large effect of loss-of-function Trem2 mutations on AD risk and on microglial function [8], argues that microglia have a protective function that lowers the incidence of AD. Hansen et al [16] synthesize the findings from disparate approaches on microglia, by proposing that microglia can compact Aβ aggregates in dense core plaques and shield them off from neurons. Aging or genetic susceptibility (*e.g.* Trem2 deficiency) can lead to inadequate microglial function and to a decrease in amyloid encystment. This results in increased amyloid toxicity and tau occurrence [6, 20, 21]. Microglia can engulf and remove synapses, and thus microglial changes may modulate neurodegenerative processes. Previous studies have attempted to elucidate the interactions between all these AD lesions using transgenic mice overexpressing human Aβ or tau (with or without frontotemporal dementia mutations) [3, 14, 26]. Over the last decade, new paradigms were established to induce widespread Aβ and tau pathologies via the intracerebral injection of human AD brain extracts in mice. These models provide a unique opportunity to reassess relationships between

AD core lesions and downstream neurodegenerative processes. In this study, we inoculated crude AD brain homogenates into mice with high Aβ production. This modulated both amyloid and tau lesions and induced synaptic loss and cognitive impairments. The extent of synaptic loss and subsequent cognitive impairment was associated with the severity of tau lesions and to lower microglial load, but not to amyloid accumulation. These results reinforce the major contribution of tau to AD-related neurodegenerative processes and indicate that in a setting that is not based on genetic disruption of microglial function (*e.g.* Trem2 or other genetic mutations) microglial activity may protect against synaptic loss.

Results

Different AD brain homogenates induce different cognitive alterations

We prepared two brain homogenates from sporadic AD patients, with each homogenate consisting in a combination of brain extracts from patients with either a rapidly evolving form of AD (rpAD defined by a rapid clinical decline and a disease duration from 6 months to 3 years) or patients with forms of AD that evolved more slowly (clAD, disease duration of 5 to 8 years). A third homogenate, considered as a control, was prepared from non-demented individuals (Ctrl). Selected AD patients had similar Braak and Thal stages and their characteristics are presented in Suppl. Table 1 and Suppl. Fig. 1-2. The amounts of amyloid, tau and neuroinflammatory proteins slightly differed between the brain homogenates, as the rpAD homogenate displayed more $A\beta_{42}$, total tau and phospho-tau181, but less $A\beta_{38}$ and $A\beta_{40}$ than the clAD one (Suppl. Fig. 2a-l). Iba1 and GFAP levels were similar in the two AD homogenates (Suppl. Fig. 2m-o).

Brain homogenates were inoculated bilaterally (2 µl/site) in the dorsal hippocampus (CA1) of 2-month-old $APP_{swe}/PS1_{de9}$ mice (n_{Ctrl}=15, n_{clAD}=15, n_{rpAD}=20 mice euthanized at 8 months post-inoculation (mpi), and n_{Ctrl}=11, n_{clAD}=14, n_{rpAD}=12 mice euthanized at 4 mpi). At this age, mice produce high levels of Aβ leading to amyloid plaques at around 4 months of age [11]. This model expresses the endogenous murine tau protein isoforms and is not transgenic of any human tau. Inoculated mice were evaluated

using a battery of behavioral tests at 8 mpi. An additional group of Ctrl-inoculated wild-type (WT) littermates was used as controls. Mice were evaluated in an object-recognition task on a V-maze test during 3 days (Fig. 1). Following the habituation phase in an empty arena on day 1, two identical objects were added to the maze on day 2, while one of them was eventually removed and replaced by a novel object on day 3. Mice from each group showed similar exploratory activity, as suggested by comparable interest in the two identical objects during the training phase on day 2 ($p>0.05$; Kruskal-Wallis with Dunn's multiple comparisons, Fig. 1a), and similar distance travelled throughout the three days of test (for the days: $F_{(1.75, 89.47)} = 91.97$, $p<0.0001$; for the groups: $F_{(3, 51)} = 0.89$, $p=0.45$; two-way repeated measures ANOVA with the Geisser-Greenhouse correction and Dunnett's multiple comparisons, Fig. 1b). During the novel object recognition evaluation on day 3, rpAD mice spent less time exploring the novel object, leading to a significantly lower discrimination index, compared to WT and $APP_{swe}/PS1_{dE9}$ clAD or Ctrl-inoculated mice (respectively, $p=0.0018$, 0.0082 and 0.0007; Kruskal-Wallis with Dunn's multiple comparisons (Fig. 1c)). These data suggest that rpAD brain inoculation leads to novel object recognition deficits, compared to clAD and Ctrl brain inoculations. Spatial memory was then assessed using the Morris water maze test (Suppl Fig. 3a-c). During the training phase, no difference was observed between the groups suggesting that Ctrl, clAD and rpAD brain inoculations do not differentially impact spatial learning abilities in $APP_{swe}/PS1_{dE9}$ mice (Suppl. Fig. 3a-b). Spatial memory retention was then evaluated 72 hours after the last training test. All groups performed as well as the WT group by spending more time in the target quadrant than in the opposite one, suggesting that spatial memory is not impaired in $APP_{swe}/PS1_{dE9}$ Ctrl or AD-inoculated mice (Suppl. Fig. 3c). Moreover, the time spent both in the target quadrant and in the opposite one was significantly different from the theoretical value of 15 seconds, which corresponds to 25% of the trial duration, supporting the idea that all groups successfully memorized the platform location (Suppl. Fig. 3c). Anxiety levels were also evaluated using the general aversion of rodents to open spaces in the elevated plus maze test, which is plus-shaped apparatus with two open and two enclosed arms. The different groups did not display differences in the distance travelled, the time spent leaning over the maze, as well as the time spent

in open and enclosed arms or at their intersection in the center of the arena (Suppl. Fig. 3d-f, $p>0.05$; Kruskal-Wallis with Dunn's multiple comparisons). These results suggest that anxiety levels are neither impacted by the $APP_{swe}/PS1_{dE9}$ phenotype, nor by the intracerebral inoculation of AD brains at 8 mpi. No difference in cognitive performance was observed at 4 mpi (Suppl. Fig. 4a-c).

INOCULATION OF DIFFERENT AD BRAIN HOMOGENATES LEADS TO DIFFERENT LEVELS OF SYNAPTOTOXICITY

Synaptic density was then evaluated in the hippocampus (CA1) and the perirhinal/entorhinal cortex of inoculated mice at 8 mpi, using a double immunolabeling of presynaptic (Bassoon) and postsynaptic (Homer) markers. The amount of colocalized punctas, an indicator of synaptic density, was decreased by 30 % and 26% in rpAD mice compared to Ctrl and clAD mice respectively in the hippocampus (Fig. 2a, respectively $p=0.0011$ and 0.037; Kruskal-Wallis with Dunn's multiple comparisons). In the perirhinal/entorhinal cortex, lower synaptic density was observed in the rpAD group compared to the Ctrl group but not to the clAD group (Fig. 2b, respectively $p=0.001$ and 0.13; Kruskal-Wallis with Dunn's multiple comparisons). No difference in synaptic density was found between the Ctrl and clAD groups (Fig. 2a-b). A decrease in the PSD95/synaptophysin ratio assessed by western blots also suggests synaptic alterations in the hippocampus of rpAD mice compared to Ctrl-inoculated animals (Fig. 2c-d). At 4 mpi, synaptic density evaluation did not reveal any differences between the groups (Suppl. Fig. 4d-e).

AD BRAIN INOCULATION ACCELERATES AB PLAQUE DEPOSITION AND INDUCES TAU ACCUMULATION CLOSE TO THE INJECTION SITE IN $APP_{SWE}/PS1_{DE9}$ MICE

At 8 mpi, AD brain inoculation led to an increase in amyloid plaque deposition in the hippocampus (immunostained with the 4G8 antibody, Fig. 3a-c, 3g) and in the region surrounding the alveus (Fig. 3d-f, 3h), compared to Ctrl brain (respectively for clAD and rpAD brains, $p=0.0005$ and $p<0.0001$ in the hippocampus, $p<0.0001$ and $p<0.0001$ in the alveus; Kruskal-Wallis with Dunn's multiple comparisons). The same changes were found at 4 mpi (Suppl. Fig. 4f-g). Soluble forms of amyloid were also quantified

in the hippocampus by western blots after Aβ extraction. No differences in soluble or membrane-associated Aβ oligomers were found between the ADs and Ctrl groups at 8 mpi (Suppl Fig 5a-d).

Three types of tau lesions occur in AD patients: neuropil threads, neurofibrillary tangles and tau-positive aggregates surrounding Aβ deposits leading to neuritic plaques. In this study, AD-like neuropil threads (NTs) (Fig. 4a), neurofibrillary tangles (NFTs) (Fig. 4b-e) and neuritic plaques (NPs) (Fig. 4f) were all recapitulated in AD-inoculated $APP_{swe}/PS1_{dE9}$ mice. At 8 mpi, compared to the Ctrl brain homogenate, the intrahippocampal inoculation of AD brain homogenates led to an overall increase in tau lesions in the hippocampus (Fig. 4g-i, 4m; $p=0.001$ and $p<0.0001$ respectively for clAD and rpAD mice; Kruskal-Wallis with Dunn's multiple comparisons) and in the alveus (Fig. 4j-l, 4p; $p=0.0035$ and $p<0.0001$ respectively for clAD and rpAD mice; Kruskal-Wallis with Dunn's multiple comparisons), as revealed by an AT8-positive immunostaining directed against hyperphosphorylated tau. The same trends, although to a lesser extent, were reported at 4 mpi (Suppl. Fig. 4i-j). In AD-inoculated mice, AT8-positive NTs were induced both in the hippocampus (Fig. 4n, $p=0.0005$ and $p<0.0001$ in clAD and rpAD mice, respectively) and the alveus (Fig. 4q, $p=0.0036$ and $p<0.0001$ in clAD and rpAD mice, respectively) whereas Ctrl-inoculated animals did not present these lesions. Moreover, AT8-positive NFTs were increased in the hippocampal hilus (Fig. 4o, $p=0.001$ and $p<0.0001$ in clAD and rpAD mice, respectively) of AD-inoculated mice as opposed to Ctrl-inoculated animals at 8 mpi.

AT100 positive labeling was also observed in the forms of NTs (Suppl. Fig. 6a, arrow heads) and NFTs (Suppl. Fig. 6a, arrow). Overall quantification of the AT100 staining showed increased labeling in the alveus of AD-inoculated mice but not in the hippocampus (Suppl. Fig. 6b-c, $p=0.0007$ and 0.092 respectively, Mann-Whitney test). Gallyas silver staining revealed neuropil thread labelling (Suppl. Fig. 6d) as well as amyloid plaques (Suppl. Fig. 6e). No quantification was performed as this technique reveals both tau and amyloid lesions.

Amyloid lesions can facilitate the occurrence of tau pathology notably in neurites and lead to neuritic plaques. Indeed, the experimental inoculation of tau from sarkosyl-insoluble AD brain extracts in mice

with high amyloid plaque load induces NPs [17]. Consistently with these results, we detected NPs in the hippocampus of AD-inoculated mice (Fig. 5b-c, 5e-f). Unexpectedly, NPs were also detected in Ctrl-inoculated mice (Fig. 5a, 5d). Quantification showed that NP count was similar in all groups (Fig. 5h). To further evaluate if human brain inoculation was necessary to induce these lesions, we performed an AT8 staining in old non-inoculated $APP_{swe}/PS1_{de9}$ mice and also observed neuritic plaques (Fig. 5g).

Interindividual heterogeneity was observed for both Aβ and tau lesions. We took advantage of this heterogeneity to assess the relationships between Aβ and tau pathologies. In the hippocampus, amyloid load was correlated to NTs (Fig. 6a, $r_{spearman\text{-}hip}=0.78$, $p<0.0001$), NFTs (Fig. 6b, $r_{spearman\text{-}hip}=0.79$, $p<0.0001$) and to global tau pathology (Fig. 6c, $r_{spearman\text{-}hip}=0.72$, $p<0.0001$) but not to NPs (Fig. 6d, $r_{spearman\text{-}hip}=0.13$, $p=0.39$). Thus, the severities of amyloid and tau lesions at the inoculation site were related to one another. It is however difficult to establish whether this association only results from the concomitant inoculation of both amyloid and tau, or whether it reflects a direct impact of Aβ on tau pathology induction.

Inoculation of AD brain extracts induces Tau but not Ab spreading in APPswe/PS1de9 mice

We then evaluated the spreading of Aβ and tau lesions from the hippocampus to connected perirhinal/entorhinal brain regions (Fig. 7a-b). Amyloid load was similar in the perirhinal/entorhinal cortex of rpAD, clAD and Ctrl mice (Fig. 7c-e, 7i, $p<0.05$; Kruskal-Wallis' test). Aβ detected in the perirhinal/entorhinal cortex may thus only reflect the endogenous expression of the peptide in the $APP_{swe}/PS1_{dE9}$ model. Conversely, overall hyperphosphorylated tau lesions (AT8-positive) were clearly increased in the perirhinal/entorhinal cortex of AD brain inoculated animals compared to Ctrl-inoculated ones (Fig. 7f-h, 7j, $p=0.0007$ and $p=0.0002$, respectively for clAD and rpAD mice; Kruskal-Wallis with Dunn's multiple comparisons). Moreover, NFTs and NTs were also detected in the perirhinal/entorhinal cortex of AD-inoculated mice but not in Ctrl-inoculated animals (Fig. 7k, NTs accumulation for clAD and rpAD mice, $p=0.0003$ and $p=0.0002$; Fig. 7l, NTFs accumulation for clAD and rpAD mice, $p=0.005$ and $p<0.0001$; Kruskal-Wallis with Dunn's multiple comparisons). These lesions

were mainly found in the external layers II and III of the cortex (Fig 7f-h) that project to the dentate gyrus via the perforant pathway and to the CA1 region via the temporammonic pathway, respectively. On the contrary, internal layers (*e.g.* layers V-VI) that receive projections from the CA1 region were not labelled. Other cortical regions such as the visual cortex also displayed NFTs, NTs and NPs in clAD and rpAD mice (Suppl. Fig. 7a-b). Neuritic plaque accumulation was increased in the perirhinal/entorhinal cortex of rpAD-inoculated mice compared to Ctrl mice (Fig. 7m ,$p=0.038$; Kruskal-Wallis with Dunn's multiple comparisons). As in the hippocampus, AT100 revealed tau lesions in the perirhinal/entorhinal cortex (Suppl. Fig. 8a-b) and a statistical difference in AT100-positive staining was detected between the ADs and Ctrl groups ($p=0.005$; Mann-Whitney test) (Suppl. Fig. 8c). Gallyas staining was also positive for tau lesions (Suppl. Fig. 8d-e) and amyloid plaques (Suppl. Fig. 8d, 8f) in this region. No spreading of amyloid nor tau lesions was reported by 4 mpi (Suppl. Fig. 4h, 4k) although lesions were observed next to the inoculation site. Altogether data at 4 and 8 mpi suggest that tau lesions gradually spread through the brain in a time-dependent manner.

Tau spreading is associated to tau and Ab lesions at the inoculation site but not in projecting areas

All of tau pathological markers in the perirhinal/entorhinal cortex were strongly correlated to tau markers in the hippocampus (Fig. 8a-d, $r_s=0.90$ to 0.67 depending on the marker, $p<0.0001$). This suggests that AD brain inoculation in the CA1 region induces the seeding and spreading of pathological tau to anatomically and functionally connected neurons (Fig. 7b, 7f-h). Tau lesions in the perirhinal/entorhinal cortex were also correlated to amyloid load in the hippocampus (NTs: Fig. 8f, $r_{spearman\text{-}hip}=0.72$, $p<0.0001$; NFTs: Fig. 8g, $r_{spearman\text{-}hip}=0.74$, $p<0.0001$; global tau pathology: Fig. 8e, $r_{spearman\text{-}hip}=0.64$, $p<0.0001$; NPs: Fig. 8h, $r_{spearman\text{-}hip}=0.42$, $p=0.004$). Unexpectedly, none of tau perirhinal/entorhinal lesions were correlated to amyloid load in this same region (Fig. 8i-l, $p>0.05$ Spearman's correlation).

TAU BUT NOT AB PATHOLOGY IS ASSOCIATED TO DECREASED SYNAPTIC DENSITY AND TO LOW COGNITIVE SCORES

To further evaluate the origins of AD-like functional and synaptic heterogeneity, we assessed the relationships between synaptic density, cognitive scores, tau and amyloid pathologies. Synaptic density was inversely correlated to global tau pathology (Fig. 9a, 9d, $r_{spearman\text{-}hip}$=-0.37, p=0.008 and $r_{spearman\text{-}P/EC}$=-0.32, p=0.03), NTs (Fig. 9e, $r_{spearman\text{-}P/EC}$=-0.43, p=0.003), NFTs (Fig. 9f, $r_{spearman\text{-}P/EC}$=-0.38, p=0.011) and NPs (Fig. 9g, $r_{spearman\text{-}P/EC}$=-0.50, p=0.0005). In addition, tau pathology in both the hippocampus and the perirhinal/entorhinal cortex was also correlated to cognitive impairment in the V-maze test (global tau pathology (Fig. 10a-b, $r_{spearman\text{-}hip}$=-0.35, p=0.021 and $r_{spearman\text{-}P/EC}$=-0.42, p=0.0059); NTs (Fig. 10c-d, $r_{spearman\text{-}hip}$=-0.44, p=0.0039 and $r_{spearman\text{-}P/EC}$=-0.36, p=0.022); NFTs (Fig. 10e-f, $r_{spearman\text{-}hip}$=-0.34, p=0.032 and $r_{spearman\text{-}P/EC}$=-0.40, p=0.012)). These data suggest that tau contributes to synaptic and cognitive alterations. Synaptic density was not correlated to amyloid load in the hippocampus nor in the perirhinal/entorhinal cortex (Fig. 9b, 9h, p>0.05). Amyloid load in the hippocampus, but not in the perirhinal/entorhinal cortex, was however negatively correlated to cognitive changes in the V-maze (Fig. 10g-h, $r_{spearman\text{-}hip}$=-0.48, p=0.001 and $r_{spearman\text{-}P/EC}$=-0.17, p=0.29).

REDUCED MIGROGLIAL ACTIVATION IS ASSOCIATED WITH SYNAPTIC LOSS AND COGNITIVE ALTERATIONS

Neuroinflammation was assessed by measuring microglial (Iba1-staining, Fig. 11) and astrocytic (GFAP staining, Suppl. Fig. 9) loads. Quantification revealed similar levels of Iba1 (Fig. 11a-b) and GFAP (Suppl. Fig. 9a-b) staining areas in the clAD, rpAD and Ctrl groups. However, as for tau and Aβ, a strong interindividual heterogeneity was observed. In each group, some animals displayed high Iba1 labelling (Fig. 11c-e, 11i-k) with abundant activated microglia characterized by beading with spheroidal swellings of the processes (Fig. 11o-p, arrow heads) and enlarged cell body with dystrophic ramifications (Fig. 11o-p, arrows) [28]. These activated cells formed microglial clusters surrounding Aβ plaques (Fig. 11q). In contrast, some mice had low Iba1 labelling (Fig. 11f-h, 11l-n) with highly ramified microglia, both close to and far from amyloid plaques (Fig. 11r and 11s respectively), which is

consistent with a non-activated phenotype. A positive correlation was reported between Iba1 staining and synapses in the hippocampus (Fig. 9c, $r_{spearman\text{-}hip}$=0.50, p=0.0002) and the perirhinal/entorhinal cortex (Fig. 9i,$r_{spearman\text{-}P/EC}$=0.44, p=0.0018), but no relationship between GFAP staining and synapses was observed in these regions (not shown). Iba1 staining in the hippocampus and perirhinal/entorhinal cortex was also correlated with cognitive scores in the object recognition test (Fig. 10i-j, $r_{spearman\text{-}hip}$=0.34, p=0.028; $r_{spearman\text{-}P/EC}$=0.45, p=0.003). Taken together, these results suggest that reduced microglial activation is associated to synaptic loss and cognitive alterations. No direct relationship was found between Iba1 staining and Aβ or tau (not shown).

Discussion

Based on the intracerebral inoculation of crude AD brain homogenates into mice with high Aβ production, we produced a highly pathologically relevant AD model which develops tau lesions that spread in the brain, amyloid plaques, synaptic alterations and cognitive impairments. In humans, tau lesions spread into amyloid-rich isocortical regions during the evolution from Braak IV to Braak V stages [4, 9]. This timeframe is critical as it is associated to the transition of the disease into a clinical phase. Our model may reflect this period of AD pathology.

NFTs and NTs were only induced in $APP_{swe}/PS1_{dE9}$ mice inoculated with human AD brains. This suggests that pathological misfolded tau seeds are required to trigger NFT and NT formation. These lesions spread from the inoculated site to connected brain regions such as the perirhinal/entorhinal cortex. NPs were detected both in AD-inoculated and Ctrl-inoculated mice as well as in aged non-inoculated mice. Neuritic tau lesions have already been reported in Aβ plaque-bearing mice without AD brain inoculation or tau overexpression [22]. In humans, different forms of amyloid plaques, including non-Aβ ones, can induce tau lesions in surrounding neurites [10]. Taken together, these results highlight that amyloid plaques create a microenvironment that induces the occurrence and amplification of tau lesions. Amyloid load was increased in the hippocampus and surrounding areas following AD brain intrahippocampal inoculation. This local increase in amyloid load is consistent with several studies [7,

12]. Amyloid spreading has been described following the inoculation of Aβ-enriched brain extracts from mice [33]. We did not reproduce these results as, unlike tau, Aβ did not spread to the perirhinal/entorhinal cortex. This spreading effect might be hidden in our $APP_{swe}/PS1_{de9}$ mice that spontaneously develop high amyloid plaque load over time.

In addition to amyloid and tau, our study focused on synaptic and cognitive impairments. We provided the first experimental evidence that the intracerebral inoculation of different AD brain homogenates can induce different cognitive alterations and synaptic loss, including in regions where tau has spread. This suggests that part of AD heterogeneity may be reproduced although its origin remains to be established. Indeed, while the rpAD brain homogenate presented more phospho-tau pathology (pT181) and $A\beta_{42}$ than the clAD brain homogenate, these differences did not lead to differential Aβ, tau or neuroinflammation levels in the inoculated animals. It is however well-established that dynamic interactions occur between these lesions and can interfere with normal cognitive function. Therefore, to further assess whether synaptic and cognitive impairments were related to amyloid, tau or neuroinflammation, we took advantage of interindividual heterogeneity in mice. We exploited gradients of Aβ, tau and neuroinflammatory pathologies resulting from this variability to assess relationships between lesion loads. The strong association, at 8 mpi, in both the hippocampus and the perirhinal/entorhinal cortex between tau pathology and synaptic deficits or cognitive impairments suggest that tau contributes to synaptic alterations. This is consistent with recent studies [6].

The second marker strongly linked to synaptic loss and cognitive impairment was microglia. Proliferation and activation of microglia, concentrated around amyloid plaques, are prominent features of AD [16]. Increased microglial activation has been linked to synaptic alterations in amyloid-bearing models [31]. Increased microglial activity is also linked to synaptic impairments in mouse models overexpressing human tau [6]. However, human genetic evidence, exemplified by the large effect of loss-of-function Trem2 mutations on AD risk and on microglial function, argues that microglia have a protective function that lowers the incidence of AD [16]. In our study, we used $APP_{swe}/PS1_{de9}$ mice with a high microglial activity in relation with their high amyloid load. However, some animals

displayed low Iba1 labelling with highly ramified microglia, which is consistent with a non-activated phenotype. The association of lower microglial loads with reduced synaptic density and cognitive scores suggests for the first time in a model that is neither based on microglia mutation (*e.g.* Trem 2) nor based on tau overexpression, that low microglial activity is associated to synaptic and cognitive alterations and argues that activated microglia may have a protective function. We did not find any direct relationships between microglial activation and amyloid or tau lesions and can thus not propose a hypothesis to explain the reduced microglia load found in some animals. Previous studies showed that soluble phospho-tau drive microglia degeneration [28]. This could be one possible explanation for the microglia changes that we observed, but we can not rule out that inoculated brain samples contained factors that regulated microglial state.

One unexpected finding of our study is the weak association between Aβ and synaptic changes. This does not rule out the well-described link between Aβ and synaptic alterations. In our experiments, we studied Aβ plaque-bearing mice and it is possible that Aβ-related changes of synaptic function occurred in all experimental groups. Several studies have suggested that microglia encyst amyloid and prevent its toxicity [5]. The synaptotoxicity that we observed in association with a reduction of microglia load, could thus be related to a decreased amyloid enkystment leading to its increased toxicity. Further study are required to assess this hypothesis. A figure that recapitulates possible links between the different markers evaluated in this study is presented in Suppl. Fig. 10. Reduced microglial activity seems to be central to the induced synaptic pathology in this scheme.

A major limitation in AD research is the lack of animal models that faithfully reproduce AD hallmarks as seen in humans. The intracerebral inoculation of human brain extracts in mice provides pathologically relevant AD models. The induction of tau aggregates in wild-type mice has previously been reported following the injection of either AD brain homogenates [5] or highly aggregated human wild-type tau from sarkosyl-insoluble AD brain extracts [1, 15]. Moreover, mice with high Aβ production inoculated with sarkosyl-insoluble brain extracts from AD brains display both amyloid and tau pathologies. For the first time here, we used a strategy based on the inoculation of crude AD brain

homogenates into mice with high Aβ production to induce tau lesions, amyloid plaques and downstream events including synaptic loss and cognitive impairments. Altogether, this model will be helpful to assess interactions between AD core lesions and neurodegenerative processes, as well as to evaluate new therapies targeting multiple AD hallmarks. It is critical to outline that our experimental paradigm based on inoculation of pools of brains from patients with rapidly evolving or classical forms of AD does not allow to conclude on a direct relationship between these forms of the disease and the induced pathologies in mice or to interpret our results in term of strain effects. Further studies should be performed, based on inoculation of well characterized brain extracts from single patients to study strain effects. Here pools where only used to artificially create variability within inoculated samples and we propose that this could be a novel approach to study AD-related heterogeneity in animal models.

As a conclusion, we showed that intracerebral injection of human AD brain extracts into an Aβ plaque–bearing mouse model that does not overexpress tau can recapitulate amyloid and tau lesions. Inoculation of different human AD brain extracts to mice led to lesional heterogeneity including for synaptic loss and cognitive impairments. Synaptic loss and cognitive deficits were associated with the severity of tau lesions which highlight the contribution of tau to synaptic pathology in a model that does not rely on genetic manipulation of tau protein. Synaptic loss and cognitive deficits were also associated to lower microglial load. These data observed in a model that is not based on genetic disruption of microglial function (*e.g.* Trem2 or other genetic mutations) indicate that microglial activity may protect against synaptic loss. This finding may have potential applications, including recommendations to limit anti-inflammatory therapies in subjects at risk for Alzheimer's disease.

Material and methods

HUMAN BRAIN COLLECTION AND CHARACTERIZATION

HUMAN BRAIN SAMPLES

Frozen brain samples (parietal cortex) from clinically different AD patients (four patients with classical slowly evolving forms of AD and four with a rapidly evolving form of AD) and two age-matched control individuals were collected from a brain donation program of the GIE NeuroCEB and the CNR-prion brain banks. Consent forms were signed by either the patients themselves or their next of kin in their name, in accordance with French bioethics laws. The rapidly evolving AD cases (rpAD) are characterized by a rapid cognitive decline and a disease duration of 6 months to three years. No case of hippocampal sclerosis was reported and all brain samples (Ctrl, clAD, rpAD) were PrPSc negative. clAD and rpAD brain samples were also negative for α-synuclein and TDP-43.

NEUROPATHOLOGICAL CHARACTERIZATION

All brain tissues were assessed by immunohistochemistry, as previously described in Gary et al. 2019 [12]. Briefly, 4-µm-thick paraffin sections were cut, deparaffinized in xylene, successively rehydrated in ethanol (100, 90, and 70%) and rinsed under running tap water for 10 min before immunohistological staining. They were then incubated in 99% formic acid for 5 min, quenched for endogenous peroxidase with 3% hydrogen peroxide and 20% methanol, and washed in water. Sections were blocked at room temperature for 30 min in 4% bovine serum albumin (BSA) in 0.05 M tris-buffered saline, with 0.05% Tween 20, pH 8 (TBS-Tween, Sigma). They were then incubated overnight at +4 °C with the 6F3D anti-Aβ antibody (Dako, 1/200), polyclonal anti-tau antibody (Dako, 1/500), monoclonal anti-alpha-synuclein (LB509, Zymed, 1/250), polyclonal anti-TDP43 (Protein Tech Group, 1/1000) routinely used for β-amyloid, tau, alpha-synuclein and TDP43 detection, respectively. Sections were further incubated with a biotinylated secondary antibody for 25 min at room temperature, and the presence of the secondary antibody was revealed by a streptavidin–horseradish peroxidase

conjugate using diaminobenzidine (Dako, Glostrup, Denmark). Sliced were counterstained with Harris hematoxylin.

PROTEIN EXTRACTION

For tau protein extraction, brain homogenates were sonicated on ice for 5 min, centrifuged for 5 min at 3,000 x g at +4 °C, diluted in 20 mM Tris/2% SDS and sonicated on ice for 5 min. For Aβ, Iba1 and GFAP protein extractions, brain homogenates were sonicated (6 strokes, cycle 0.5, 30% amplitude) in a lysis buffer at a final concentration of 50mM Tris-HCl pH 7.4, 150 mM NaCl, 1% Triton-X-100 supplemented with 1X protease inhibitors (cOmplete™ Mini, EDTA-free Protease Inhibitor Cocktail, Roche) and 1/100 diluted phosphatase inhibitors (Phosphatase Inhibitor Cocktail 2, Sigma-Aldrich). Samples were centrifuged at 20,000 x g for 20 minutes at +4°C and the supernatant was collected for further use. Extracted samples were stored at -80°C after evaluation of total protein concentration by a BCA assay (Pierce™).

WESTERN BLOTS

For tau characterization, samples were diluted to 1 µg/µL, diluted in 2X lithium dodecyl sulfate (LDS, Thermo Fisher Scientific) buffer with reducers and heated at +100 °C for 10 min. 15 µg of samples were loaded on a 12% Bis-TrisCriterion™ gel (Bio-Rad) and migrated in MOPS buffer for 1 hour at 165 V on ice. After protein transfer on nitrocellulose sheets, migration and quality of the transfer were checked with a ponceau S staining. The membrane was saturated for 1 hour at room temperature, and was then incubated with the AT100 (pT212-pS214, Life technologies MN1060), 2H9 (pS422, 4BioDx 4BDX-1501), tau-Nter (12-21, LB lab-made) or tau-Cter (clone 9F6, LB lab-made) antibodies overnight at + 4 °C. A peroxidase coupled secondary anti-rabbit or anti-mouse antibody was then applied for 45 min at room temperature. Immunoblotting was revealed by ECL. GAPDH (Sigma 9545) was used as a loading control. For Iba1 and GFAP evaluations, extracted samples were denatured at +90°C for 5 min in a buffer containing 1X LDS (NuPAGE® LDS sample buffer, Invitrogen) and DTT 1X (NuPAGE® sample reducing agent, Invitrogen). 10 µg of denatured protein were loaded per well. Samples and molecular

weight marker (Bio-Rad Precision Plus Protein™ Dual Color standards) were loaded on 4-20% Criterion™ TGX™ gels (Bio-Rad) and migration was performed in a 1X tris-glycine buffer (Bio-Rad) at 120V for 1 hour. Proteins were then transferred to a nitrocellulose membrane using the Trans-Blot® Turbo™ (Biorad) system. Migration and quality of the transfer were checked with a ponceau S staining. The membrane was then blocked with a TBS/0.1%Tween, 5% milk solution for 1 hour at RT, and incubated with the primary antibody Iba1 (Wako 1919741, 1/2000), GFAP (Dako Z0334, 1/5000) or actin (Sigma A2066, 1/5000) diluted in saturation buffer overnight at +4°C. After washing in TBS/0.1%Tween solution, the membrane was incubated with the appropriate secondary HRP-conjugate antibody diluted to 1/5000 in TBS/0.1%Tween for 1h at RT. The chemiluminescent signal was revealed using the Clarity western ECL (Bio-Rad) kit and the Chemidoc™ MP (Bio-Rad) imaging system. Protein band intensities were quantified on the ImageJ software and normalized by the actin expression level.

ELISA QUANTIFICATIONS

For amyloid protein quantification, all assay-specific material (pre-coated microtiter plate, buffers, antibodies, standard solutions) was provided in the V-PLEX kit Aβ Peptide Panel 1 (6E10) (MSD®). Human brain homogenates were diluted to 1/5 (Ctrl samples) or 1/10 (clAD and rpAD samples) in the dilution buffer. As described in the manufacturer's protocol, the microtiter plate was blocked for 1 hour at RT with the appropriate buffer. After washing, 25µl of detection antibody and 25µl of diluted sample or standard were added in duplicate to the wells and incubated under continuous agitation for 2h at RT. Wells were washed and 150µl of reading buffer was added. Plate reading was performed with the MSD Sector Imager 2400 (model 1200) multiplex assay system. $A\beta_{1-38}$, $A\beta_{1-40}$ and $A\beta_{1-42}$ quantifications were performed with the Discovery Workbench 4.0 MSD® software. Tau protein quantifications (total tau and phosphot-tau181) were perfomed according to the manufacturer's protocol. Briefly, brain homogenates were diluted to 1/100 and 1/200 in the provided dilution buffer. 50µl of standards or samples, as well as 50µl of detection antibody solution were added to wells and incubated for 14 hours at +4°C. After washing, 100µl of 1X anti-rabbit IgG HRP solution was added for

a 30 min incubation period at RT. 100µl of stabilized chromogen were then added to each well for 30 min at RT, in the dark. The reaction was stopped by adding 100µl of Stop solution and the plate was read at 450 nm within the hour. Data were analyzed with GraphPad Prism 7 using the 4PL method. All samples were tested in duplicates.

HOMOGENATE PREPARATION

Parietal cortex samples were individually homogenized at 10% weight/volume (w/v) in a sterile 1X Dulbecco's phosphate buffer solution in CK14 soft tissue homogenizing tubes at 5000 rpm for 20 sec (Precellys®, Bertin technologies). Brain homogenates were then sonicated on ice for 5 sec at 40% amplitude and centrifuged at 3000g for 5 min at +4°C. The supernatant was aliquoted in sterile polypropylene tubes and stored at − 80 °C until use.

TRANSGENIC MICE

All $APP_{swe}/PS1_{de9}$ mice on a C57BL/6J background were born and bred in our center (Commissariat à l'Energie Atomique, centre de Fontenay-aux-Roses; European Institutions Agreement #B92-032-02). This model expresses a chimeric mouse/human APP with the Swedish mutation and a human presenilin-1 lacking exon 9 [19], leading to an increase in amyloid production. Genotyping was performed after DNA extraction with the KAPPA Mouse Genotyping (Kappa Biosystems) kit and PCR amplification using the following primers: APP_F: 5' - AGG ACT GAC CAC TCG ACC AG - 3', APP_R: 5' - CGG GGG TCT AGT TCT GCA T - 3', internal control_F: 5' - CTA GGC CAC AGA ATT GAA AGA TCT - 3', internal control_R: 5' - GTA GGT GGA AAT TCT AGC ATC ATC C - 3'. Electrophoresis was performed on a 3% agarose gel. All animals were randomly assigned to the experimental groups. Males were exclusively used in this study. All experimental procedures were conducted in accordance with the European Community Council Directive 2010/63/UE and approved by local ethics committees (CEtEA-CEA DSV IdF N°44, France) and the French Ministry of Education and Research (A17_083 authorization).

PREPARATION OF BRAIN SAMPLES AND STEREOTAXIC SURGERY

10% Ctrl, clAD or rpAD individual brain homogenates were thawed on ice and pooled together according to their group. The three resulting pooled samples (Ctrl, clAD, rpAD) were sonicated (70% amplitude, 10 sec on/off; Branson SFX 150 cell disruptor sonicator, 3.17mm microtip probe Emerson, Bron) on ice in a sterile environment, extemporaneously before stereotaxic injection. 2 month-old $APP_{swe}/PS1_{de9}$ and wild-type littermates were anesthetized by an intraperitoneal injection of ketamine (1mg/10g; Imalgène 1000, Merial) and xylazine (0.1mg/10g; 2% Rompun, Bayer Healthcare). Local anesthesia was also performed by a subcutaneous injection of lidocain (1 µl/g; 0.5% Xylovet, Ceva) at the incision site. Mice were placed in the stereotaxic frame (Phymep) and bilateral injections of brain samples were performed in the dorsal hippocampus (AP -2 mm, DV -2 mm, L +/- 1 mm from bregma). Using 34-gauge needles and Hamilton syringes, 2µl of sample were administered at a 0.2µl/min rate. After the injection, needles were kept in place for 5 more minutes before removal and the incision was sutured. The surgical area was cleaned before and after the procedure using povidone iodine (Vétédine, Vétoquinol). Respiration rate was monitored and body temperature was maintained at 37±0.5°C with a heating pad during the surgery. Anesthesia was reversed with a subcutaneous injection of atipamezole (0.25 mg/kg; Antisedan, Vetoquinol). Mice were placed in a ventilated heating box (25°C) and monitored until full recovery from anesthesia. Postoperative pain management consisted in paracetamol administration in drinking water (1.45ml/20ml of water; Doliprane, Sanofi) for 48 hours.

BEHAVIORAL TESTS

Mice were handled for 2 minutes per day, for 5 days prior to any test. Before each test, mice were habituated to the experimental room for 30 minutes. A battery of behavorial tests was then conducted on $APP_{swe}/PS1_{de9}$ mice eight or four months after intracerebral inoculation of the brain homogenates (at 8 and 4 mpi respectively, n_{Ctrl}=15 and 11, n_{clAD}=15 and 14, n_{rpAD}=20 and 12). Wild-type littermates injected with the Ctrl brain sample were used as controls for the tests (at 8 and 4 mpi respectively,

n_{WT}=12 and 6). The experimenter was blind to mouse groups. Between mice, the elevated plus maze and V-maze were cleaned with 10% ethanol and dried. Performances were recorded using a tracking software (EthoVision XT14, Noldus).

Elevated plus maze

The elevated plus maze is a plus-shaped apparatus placed at 50 cm above the floor. It consists in four 5cm wide and 40cm long segments, among which two are open arms (associated with a 150 lux-lighting) and two are enclosed arms (associated with a 15 lux-lighting). Mice were placed at the center of the maze facing an open arm for a 6-min trial. Distance travelled and time spent in each arm were automatically calculated by the software. The time spent leaning over the edge of open arms was scored manually.

Novel object recognition in the V-maze

The V-maze arena consisted in two 6 cm-wide, 33.5 cm-long and 15 cm-high black arms forming a V and exposed to a 50 lux-lighting. The test was divided into three phases, each one separated by 24 hours. At the beginning of each session, mice were placed at the center of the arena, *i.e.* at the intersection of the arms, exposed to a 50 lux-lighting. During the habituation phase (day 1), mice were free to explore the empty arena for 9 minutes. The distance travelled was automatically recorded as an indicator of their exploratory activity. For the training phase (day 2), two identical objects (bicolor plastic balls) were placed at the end of each arm. Exploratory activity was evaluated as the time spent exploring the objects (manually recorded) and the distance travelled during the 9-minute trial. On the test day (day 3), one familiar object (a bicolor plastic ball) was replaced by a novel one of a different shape and material (a transparent glass flask). Recognition was assessed using a discrimination index, calculated as follows:

$$Discrimination\ index = \frac{Time\ exploring\ the\ novel\ object - Time\ exploring\ the\ familiar\ object}{Total\ exploration\ time}$$

It reflects the time spent exploring each object, and therefore, the ability to discriminate a novel object from a familiar, previously explored one. A high discrimination index score reveals that mice spent

more time exploring the new object, *i.e.* had less interest in a familiar object, and suggests that their memory is not impaired.

Morris water maze

An open 122 cm-wide circular swimming arena was maintained at 22°C and exposed to a 400 lux-lighting. The test consisted of three phases during which the arena was divided into four artificial quadrants. At the end of each session, mice were dried with a heated towel before returning to their home cages. During the habituation phase (day 1), mice were trained to find a visible platform to escape from the water. To facilitate its detection, the platform was emerged 0.5 cm above the surface of the water and a colorful cue was placed on it. This phase consisted in four 60-seconds trials, with an inter-trial interval (ITI) of 20-30 minutes. For each trial, the starting point was different as well as the location of the platform. When the mice did not find the platform within the 60 seconds, they were guided to its location and were left on the plateform to rest for 30 seconds. The training phase (day 2 to 6) consisted in three daily 60-seconds trials, with 20-30 minutes ITI, for five days. For each trial, the starting point was different whereas the location of the platform remained the same. The platform was hidden 0.5 cm beneath the water surface and the cue previously placed on it was removed. Visual cues were placed around the maze so that mice could spatially navigate to the platform. When the mice did not find the platform within the 60 seconds, they were guided to its location and were left on the platform to rest for 30 seconds. All trials lasted 60 s or until the animal located the platform. Escape latency, *i.e.* the time required to find the platform, was evaluated during the habituation and the training phases to assess learning abilities. A probe test (day 7) was performed 72 hours after the last training session to assess spatial long-term memory. During this phase, the platform was removed from the maze. Mice were placed in the water for 60 seconds from a position opposite to the platform. The time spend in each virtual quadrant of the maze was recorded.

HISTOLOGY

Mice were sacrificed at 8 or 4 mpi, after the behavioural tests, with an intraperitoneal injection of a lethal dose of pentobarbital (100 mg/kg; Exagon, Axience). They were perfused intracardiacally with cold sterile 0.1M PBS for 4 minutes, at a rate of 8 ml/min. The brain was extracted and the two cerebral hemispheres were separated. The left hemisphere was post-fixed in 4% paraformaldehyde for 48 hours at +4°C, transferred in a 15% sucrose solution for 24 hours and in a 30% sucrose solution for 48 hours at +4°C for cryoprotection. Serial coronal sections of 40 µm were performed with a microtome (SM2400, Leica Microsystem) and stored at -20°C in a storing solution (glycerol 30%, ethylene glycol 30%, distilled water 30%, phosphate buffer 10%). Free-floating sections were rinsed in a 0.1M PBS solution (10% Sigma-Aldrich® phosphate buffer, 0.9% Sigma-Aldrich® NaCl, distilled water) before use.

IMMUNOHISTOCHEMISTRY

A pretreatment with 70% formic acid (VWR®) for 20 min at room temperature (RT) was performed for the 4G8 labelling, while a pretreatment with EDTA 1X citrate (Diagnostic BioSystems®) for 30 min at 95°C was performed for the AT8 and AT100 labellings. Tissues were then incubated in hydrogen peroxide H_2O_2 30% (Sigma-Aldrich®) diluted 1/100 for 20 min to inhibit endogenous peroxidases. Blocking of non-specific antigenic sites was achieved over 1 hour using a 0.2% Triton X-100/0.1M PBS (Sigma-Aldrich®) (PBST) solution containing 4.5% normal goat serum. Sections were then incubated at +4°C with the 4G8 (Biolegend 800706, 1/500), Iba1 (Wako 1919741, 1/1000) or GFAP (Dako Z0334, 1/10000) antibody diluted in a 3%NGS/PBST solution for 48h, or with the AT8 (Thermo MN1020B, 1/500) or AT100 (Thermo MN1060, 1/500) antibody diluted in a 3%NGS/PBST solution for 96h. After rinsing, an incubation with the appropriate biotinylated secondary antibody diluted to 1/1000 in PBST was performed for 1h at RT, followed by a 1h incubation at RT with a 1:250 dilution of an avidin-biotin complex solution (ABC Vectastain kit, Vector Laboratories®). Revelation was performed using the DAB Peroxidase Substrate Kit (DAB SK4100 kit, Vector Laboratories®). Sections were mounted on Superfrost Plus slides (Thermo-Scientific®). For the AT8 and AT100 labellings, a cresyl violet counterstain was

performed. All sections were then dehydrated in successive baths of ethanol at 50°, 70°, 96° and 100° and in xylene. Slides were mounted with the Eukitt® mounting medium (Chem-Lab®).

IMMUNOFLUORESCENCE

Free-floating sections were permeabilized in a 0.5% Triton X-100/0.1M PBS (Sigma-Aldrich®) solution for 15min. Slices were incubated with Bassoon (Abcam Ab82958, 1/200) and Homer (Synaptic systems 160003, 1/400) antibodies diluted in 3%BSA/PBST solution for 24 hours at +4°C. Incubation with secondary antibodies coupled to a fluorochrome (Alexa Fluor) diluted in a 3%BSA/0.1M PBS solution was then performed for 1h at RT. Sections were mounted on Superfrost Plus (Thermo-Scientific®) slides with Vectashield® mounting medium with a refractive index of 1.45.

GALLYAS SILVER STAINING

All steps were performed between 20 and 25°C. Free-floating sections were mounted on Superfrost Plus (Thermo-Scientific®) slides and dried overnight prior to Gallyas staining. Section were permeabilized by successive incubations in toluene (2x5min) followed by ethanol at 100°, 90° and 70° (2min per solution). Slides were then incubated in a 0.25% potassium permanganate solution for 15 min, in 2% oxalic acid for 2 min then in a lanthanum nitrate solution (0.04g/l lanthanum nitrate, 0.2g/l sodium acetate, 10% H2O2 30%) for 1h to reduce non-specific background. Several rinses with distilled water were performed followed by an incubation in an alkaline silver iodide solution (3.5% AgNO3 1%, 40g/l NaOH, 100g/l KI) for 2 min. The reaction was neutralized with 0.5% glacial acetic acid baths (3x1min) and sections were incubated for 20 min in a developing solution (2g/l NH4NO3, 2g/l AgNO3, 10g/l tungstosilicilic acid, 0.76% formaldehyde 37%, 50g/l anhydrous Na2CO3). Several rinses with 0.5% acetic acid (3x1min) followed by an incubation in 1% gold chloride solution for 5min were then carried out. Sections were rinsed with distilled water and the staining was fixed with a 1% sodium thiosulfate solution. All sections were then rinsed with distilled water and dehydrated for 1 to 5 min in successive baths of ethanol at 50°, 70°, 96° and 100° and in xylene. Slides were mounted with Eukitt® mounting medium (Chem-Lab®).

IMAGE ANALYSIS

IMMUNOHISTOCHEMISTRY AND GALLYAS SILVER STAINING

Z-stack images were acquired at 20× (for Iba1, AT8 and AT100 stainings, z-stacks with 16 planes, 1µm steps with extended depth of focus) using an Axio Scan.Z1 (Zeiss®). Each slice was extracted individually in the .czi format using the Zen 2.0 (Zeiss®) software. Image processing and analysis were performed with the ImageJ software. Macros were developed for each staining in order to achieve a reproducible semi-automated quantification. Images were imported with a 50% reduction in resolution (0.44 µm/pixel), converted to the RGB format and compressed in .tif format. For the 4G8 and Iba1 immunostainings, segmentation was performed through an automatic local thresholding using the Phansalkar method (radius=15). Amyloid load was evaluated after quantification of the 4G8-labelled particles between 8 and 2,000 μm^2, and normalization to the surface area of each ROI. Microglial activity was evaluated as a percentage of Iba1-positive surface area in each ROI. For the AT8 and AT100 stainings, the blue component of each image was extracted in order to remove the cresyl violet counter-staining from the analysis. An automatic local thresholding of the staining was carried out with the Phansalkar method and the severity of tau pathology was evaluated as a percentage of AT8-positive or AT100-positive surface area in each ROI. In addition for the AT8 immunostaining, a quantification of neuritic plaques and AD-like neurofibrillary tangles was performed by manual counting. A semi-quantitative analysis of neuropil threads was also performed by assigning a severity score based on the intensity and extent of AT8-positive staining in each ROI. All quantifications were performed on adjacent slices between -0.34 mm and -4.36 mm from bregma. 10 adjacent slices were analyzed for the 4G8 staining, and 5 for Iba1, AT8, AT100 and Gallyas stainings. All ROIs were manually segmented using the Paxinos and Franklin Neuro-Anatomical Atlas of Mouse Brain [24].

IMMUNOFLUORESCENCE

Images were acquired using the Leica DMI6000 confocal optical microscope (TCS SPE) with a 63x oil-immersion objective (refractive index 1.518) and the Leica Las X software. A confocal zoom of 3 and a

pinhole aperture fixed at 1 Airy were applied. Acquisition was performed in sequential mode with a sampling rate of 1024x1024 and a scanning speed of 700 Hz. Image resolution was 60 nm/pixel and the optical section was 0.896 µm. 26 separate planes with a 0.2 µm step were acquired. The excitation wavelengths were 594 nm or 633 nm. Image acquisition in the CA1 region was performed on 4 adjacent slices located between -1.82 mm and -3.28 mm from the bregma, with 2 images per slice. For the perirhinal/entorhinal cortex, 3 adjacent slices located between -3.28 mm and -4.24 mm from the bregma were analyzed, with 2 images acquired per slice. 3D deconvolution of the images was performed using the AutoQuant X3 software. The deconvoluted 8-bit images were analyzed using the ImageJ software, as described in Gilles et al [13].

BIOCHEMISTRY

The right hemisphere of the brain was dissected on ice to extract the hippocampus, which was immediately snap-frozen in liquid nitrogen and stored at -80°C. Protein extraction was performed using sterilized material and buffers supplemented with 1X protease inhibitors (cOmplete™ Mini, EDTA-free Protease Inhibitor Cocktail, Roche) and 1/100 diluted phosphatase inhibitors (Phosphatase Inhibitor Cocktail 2, Sigma-Aldrich). The extracted samples were stored at -80°C after evaluation of their total protein concentration by a BCA (Pierce™) assay.

PROTEIN SEQUENTIAL EXTRACTION FROM MOUSE BRAINS

For amyloid protein extraction, frozen samples were mechanically lysed by sonication (Branson SFX 150 cell disruptor sonicator, 3.17mm microtip probe Emerson, Bron) in 200 µl of TBS lysis buffer (Tris-Buffer Saline) at 20mM Tris-HCl, 150mM NaCl at pH 7.4, then centrifuged at 85,000 x g for 1h at +4°C. The S1 supernatant containing the soluble fraction of the amyloid protein was stored at -80°C. The pellet was resuspended in TBS/1% Triton X-100 buffer and centrifuged at 21,000g for 10 min at +4°C. The resulting supernatant S2 containing membrane-associated amyloid was stored at -80°C. For synaptic protein extraction, frozen samples were lysed on ice using a Dounce homogenizer in 200µl of lysis buffer with 0.32M sucrose and 5mM HEPES at pH 7.5. Resulting homogenates were clarified by

centrifugation at 1,000 x g for 10min at +4°C, the supernatant was removed and centrifuged at 12,000 x g for 10 min at +4°C. The resulting pellet containing the synaptosomes was resuspended in 6mM Tris/0.32M sucrose/1mM EDTA/1mM EGTA/1mM DTT buffer at pH 8.1.

WESTERN BLOTS

For amyloid and synaptic proteins quantifications, extracted samples were denatured at +90°C for 5 min in a buffer containing 1X LDS (NuPAGE® LDS sample buffer, Invitrogen) and DTT 1X (NuPAGE® sample reducing agent, Invitrogen). 10 µg of denatured protein were loaded per well. For amyloid proteins, samples and molecular weight marker (Bio-Rad Precision Plus Protein™ Dual Xtra standards) were deposited on Criterion™ XT 4-12% Bis-Tris gels (Bio-Rad) and migration was performed in the XT MES (Bio-Rad) buffer at 120V for 1 hour. For synaptic proteins, samples and standard (Bio-Rad Precision Plus Protein™ Dual Color standards) were loaded on 4-20% Criterion™ TGX™ gels (Bio-Rad), and migration was performed in a 1X tris-glycine buffer (Bio-Rad) at 120V for 1 hour. Proteins were then transferred to a nitrocellulose membrane using the Trans-Blot® Turbo™ (Biorad) system. Migration and quality of the transfer were checked with a ponceau S staining. The membrane was then blocked with a TBS/0.1%Tween, 5% milk solution for 1 hour at RT, and incubated with the primary antibody 6E10 (Biolegend 803004, 1/5000), synaptophysin (Dako M7315, 1/1000), PSD95 (Abcam Ab18258, 1/1000), actin (Sigma A2066, 1/5000) in saturation buffer overnight at +4°C. After washing in TBS/0.1%Tween solution, the membrane was incubated with the appropriate secondary HRP-conjugate antibody diluted to 1/5000 in TBS/0.1%Tween for 1h at RT. The chemiluminescent signal was revealed using the Clarity western ECL (Bio-Rad) kit and the ChemidocTM MP (Bio-Rad) imaging system. β-actin was used as a loading control. Protein band intensities were quantified on the ImageJ software and normalized by the actin expression level.

STATISTICAL ANALYSIS

Statistical analysis was performed using the GraphPad Prism software 8. Kruskal-Wallis test with Dunn' multiple comparisons were perfomed except when repeated measures were acquired in the

behavioral tasks, in which case, a two-way repeated measures ANOVA with the Geisser-Greenhouse correction and Dunnett's multiple comparisons was carried out. Wilcoxon's signed-rank test was used to compare the time spent in the Morris Water maze quadrants with the theoretical value of 15 seconds (25% of trial duration). For comparisons between AD (clAD and rpAD mice as one AD group) and Ctrl mice, Mann-Whitney tests were conducted. For correlation studies, Spearman correlation test was performed. The significance level was set at $p<0.05$. Data are shown on scattered dot plots with mean ± standard error of the mean (s.e.m).

Author contributions

S.L., A.S.H., F.P., and M.D. contributed to the study conception and design. N.N.N., C.D. provided the human brain samples. N.N.N., S.L., S.B., C.D. and S.H. characterized the human brain samples. S.L. and M.G. performed the inoculations in mice. S.L. and K.C. designed and performed cognitive evaluations, A.S.H., F.P., S.L. designed and performed the immunohistological analysis in animals. A.S.H., S.E., L.B., and S.L. performed biochemical analysis. S.L., A.S.H., and M.D. wrote the manuscript. All authors commented on previous versions of the manuscript. All authors read and approved the final manuscript.

Competing financial interests

The authors declare no competing financial interests.

References

1 Audouard E, Houben S, Masaracchia C, Yilmaz Z, Suain V, Authelet M, De Decker R, Buee L, Boom A, Leroy K, Ando K, Brion JP (2016) High-molecular-weight paired helical filaments from Alzheimer brain induces seeding of wild-type mouse tau into an argyrophilic 4R Tau pathology in vivo. Am J Pathol: https://doi.org/10.1016/j.ajpath.2016.06.008

2 Bennett DA, Schneider JA, Wilson RS, Bienias JL, Arnold SE (2004) Neurofibrillary tangles mediate the association of amyloid load with clinical Alzheimer disease and level of cognitive function. Arch Neurol 61: 378-384. https://doi.org/DOI 10.1001/archneur.61.3.378

3 Bennett RE, DeVos SL, Dujardin S, Corjuc B, Gor R, Gonzalez J, Roe PD, Frosch MP, Pitstick R, Carlson GA, Hyman BT (2017) Enhanced Tau aggregation in the presence of amyloid beta. Am J Pathol 187: 1601-1612. https://doi.org/10.1016/j.ajpath.2017.03.011

4 Braak H, Braak E (1991) Neuropathological stageing of Alzheimer related changes. Acta Neuropathol 82: 239-259. https://doi.org/10.1007/BF00308809

5 Condello C, Yuan P, Schain A, Grutzendler J (2015) Microglia constitute a barrier that prevents neurotoxic protofibrillar Abeta42 hotspots around plaques. Nat Commun 6: 6176. https://doi.org/10.1038/ncomms7176

6 Dejanovic B, Huntley MA, De Maziere A, Meilandt WJ, Wu T, Srinivasan K, Jiang ZY, Gandham V, Friedman BA, Ngu H, Foreman O, Carano RAD, Chih B, Klumperman J, Bakalarski C, Hanson JE, Sheng M (2018) Changes in the synaptic proteome in tauopathy and rescue of Tau-induced synapse loss by C1q antibodies. Neuron 100: 1322-+. https://doi.org/ 10.1016/j.neuron.2018.10.014

7 Di Fede G, Catania M, Maderna E, Ghidoni R, Benussi L, Tonoli E, Giaccone G, Moda F, Paterlini A, Campagnani I, Sorrentino S, Colombo L, Kubis A, Bistaffa E, Ghetti B, Tagliavini F (2018) Molecular subtypes of Alzheimer's disease. Sci Rep 8: 3269 https://doi.org10.1038/S41598-018-21641-1

8 Dourlen P, Kilinc D, Malmanche N, Chapuis J, Lambert JC (2019) The new genetic landscape of Alzheimer's disease: from amyloid cascade to genetically driven synaptic failure hypothesis? Acta Neuropathol 138: 221-236. https://doi.org/10.1007/s00401-019-02004-0

9 Duyckaerts C, Braak H, Brion JP, Buee L, Del Tredici K, Goedert M, Halliday G, Neumann M, Spillantini MG, Tolnay M, Uchihara T (2015) PART is part of Alzheimer disease. Acta Neuropathol 129: 749-756. https://doi.org/10.1007/s00401-015-1390-7

10 Duyckaerts C, Sazdovitch V, Ando K, Seilhean D, Privat N, Yilmaz Z, Peckeu L, Amar E, Comoy E, Maceski A, Lehmann S, Brion JP, Brandel JP, Haik S (2018) Neuropathology of iatrogenic

Creutzfeldt-Jakob disease and immunoassay of French cadaver-sourced growth hormone batches suggest possible transmission of tauopathy and long incubation periods for the transmission of Abeta pathology. Acta Neuropathol 135: 201-212. https://doi.org/10.1007/s00401-017-1791-x

11 Garcia-Alloza M, Robbins EM, Zhang-Nunes SX, Purcell SM, Betensky RA, Raju S, Prada C, Greenberg SM, Bacskai BJ, Frosch MP (2006) Characterization of amyloid deposition in the APPswe/PS1dE9 mouse model of Alzheimer disease. Neurobiol Dis 24: 516-524. https://doi.org/10.1016/j.nbd.2006.08.017

12 Gary C, Lam S, Herard AS, Koch JE, Petit F, Gipchtein P, Sawiak SJ, Caillierez R, Eddarkaoui S, Colin M, Aujard F, Deslys JP, French Neuropathology Network, Brouillet E, Buée L, Comoy EE, Pifferi F, Picq J-L, Dhenain M (2019) Encephalopathy induced by Alzheimer brain inoculation in a non-human primate. Acta Neuropathol Commun 7: https://doi.org/10.1186/s40478-019-0771-x

13 Gilles JF, Dos Santos M, Boudier T, Bolte S, Heck N (2017) DiAna, an ImageJ tool for object-based 3D co-localization and distance analysis. Methods 115: 55-64. https://doi.org/10.1016/j.ymeth.2016.11.016

14 Gotz J, Chen F, van Dorpe J, Nitsch RM (2001) Formation of neurofibrillary tangles in P301l tau transgenic mice induced by Abeta 42 fibrils. Science 293: 1491-1495. https://doi.org/10.1126/science.1062097

15 Guo JL, Narasimhan S, Changolkar L, He ZH, Stieber A, Zhang B, Gathagan RJ, Iba M, McBride JD, Trojanowski JQ, Lee VMY (2016) Unique pathological tau conformers from Alzheimer's brains transmit tau pathology in nontransgenic mice. J Exp Med 213: 2635-2654. https://doi.org/10.1084/jem.20160833

16 Hansen DV, Hanson JE, Sheng M (2018) Microglia in Alzheimer's disease. J Cell Biol 217: 459-472. https://doi.org/10.1083/jcb.201709069

17 He ZH, Guo JL, McBride JD, Narasimhan S, Kim H, Changolkar L, Zhang B, Gathagan RJ, Yue CY, Dengler C, Stieber A, Nitla M, Coulter DA, Abel T, Brunden KR, Trojanowski JQ, Lee VMY (2018) Amyloid-beta plaques enhance Alzheimer's brain tau-seeded pathologies by facilitating neuritic plaque tau aggregation. Nature Medicine 24: 29-38. https://doi.org/10.1038/nm.4443

18 Hoover BR, Reed MN, Su J, Penrod RD, Kotilinek LA, Grant MK, Pitstick R, Carlson GA, Lanier LM, Yuan LL, Ashe KH, Liao D (2010) Tau mislocalization to dendritic spines mediates synaptic dysfunction independently of neurodegeneration. Neuron 68: 1067-1081. https://doi.org/10.1016/j.neuron.2010.11.030

19 Jankowsky JL, Fadale DJ, Anderson J, Xu GM, Gonzales V, Jenkins NA, Copeland NG, Lee MK, Younkin LH, Wagner SL, Younkin SG, Borchelt DR (2004) Mutant presenilins specifically elevate the levels of the 42 residue beta-amyloid peptide in vivo: evidence for augmentation of a 42-specific gamma secretase. Hum Mol Genet 13: 159-170. https://doi.org/10.1093/hmg/ddh019

20 Lee S-H, Meilandt WJ, Xie L, Gandham VD, Ngu H, Barck KH, Rezzonico MG, Imperio J, Lalehzadeh G, Huntley MA, Stark KL, Foreman O, Carano RAD, Friedman BA, Sheng M, Easton A, Bohlen CJ, Hansen DV (2021) Trem2 restrains the enhancement of tau accumulation and neurodegeneration by b-amyloid pathology. Neuron 109: 1–19. https://doi.org/10.1016/j.neuron.2021.02.010

21 Leyns CEG, Gratuze M, Narasimhan S, Jain N, Koscal LJ, Jiang H, Manis M, Colonna M, Lee VMY, Ulrich JD, Holtzman DM (2019) TREM2 function impedes tau seeding in neuritic plaques. Nat Neurosci 22: 1217-1222. https://doi.org/10.1038/s41593-019-0433-0

22 Metaxas A, Thygesen C, Kempf SJ, Anzalone M, Vaitheeswaran R, Petersen S, Landau AM, Audrain H, Teeling JL, Darvesh S, Brooks DJ, Larsen MR, Finsen B (2019) Ageing and amyloidosis underlie the molecular and pathological alterations of tau in a mouse model of familial Alzheimer's disease. Sci Rep 9: 15758 https://doi.org/10.1038/S41598-019-52357-5

23 Nelson PT, Alafuzoff I, Bigio EH, Bouras C, Braak H, Cairns NJ, Castellani RJ, Crain BJ, Davies P, Del Tredici K, Duyckaerts C, Frosch MP, Haroutunian V, Hof PR, Hulette CM, Hyman BT, Iwatsubo T, Jellinger KA, Jicha GA, Kovari E, Kukull WA, Leverenz JB, Love S, Mackenzie IR, Mann DM, Masliah E, McKee AC, Montine TJ, Morris JC, Schneider JA, Sonnen JA, Thal DR, Trojanowski JQ, Troncoso JC, Wisniewski T, Woltjer RL, Beach TG (2012) Correlation of Alzheimer disease neuropathologic changes with cognitive status: a review of the literature. J Neuropath Exp Neur 71: 362-381. https://doi.org/10.1097/NEN.0b013e31825018f7

24 Paxinos G, Franklin KBJ (2001) The mouse brain in stereotaxic coordinates. Academic Press, City

25 Pooler AM, Noble W, Hanger DP (2014) A role for tau at the synapse in Alzheimer's disease pathogenesis. Neuropharmacology 76: 1-8. https://doi.org/10.1016/j.neuropharm.2013.09.018

26 Pooler AM, Polydoro M, Maury EA, Nicholls SB, Reddy SM, Wegmann S, William C, Saqran L, Cagsal-Getkin O, Pitstick R, Beier DR, Carlson GA, Spires-Jones TL, Hyman BT (2015) Amyloid accelerates tau propagation and toxicity in a model of early Alzheimer's disease. Acta Neuropathol Commun 3: https://doi.org/10.1186/s40478-015-0199-x

27 Salter MW, Stevens B (2017) Microglia emerge as central players in brain disease. Nature Medicine 23: 1018-1027. https://doi.org/10.1038/nm.4397

28 Sanchez-Mejias E, Navarro V, Jimenez S, Sanchez-Mico M, Sanchez-Varo R, Nunez-Diaz C, Trujillo-Estrada L, Davila JC, Vizuete M, Gutierrez A, Vitorica J (2016) Soluble phospho-tau from Alzheimer's disease hippocampus drives microglial degeneration. Acta Neuropathol 132: 897-916. https://doi.org/10.1007/s00401-016-1630-5

29 Selkoe DJ (2002) Alzheimer's disease is a synaptic failure. Science 298: 789-791. https://doi.org/10.1126/science.1074069

30 Sivanesan S, Tan A, Rajadas J (2013) Pathogenesis of abeta oligomers in synaptic failure. Curr Alzh Res 10: 316e323. https://doi.org/10.2174/1567205011310030011

31 Spangenberg EE, Lee RJ, Najafi AR, Rice RA, Elmore MRP, Blurton-Jones M, West BL, Green KN (2016) Eliminating microglia in Alzheimer's mice prevents neuronal loss without modulating amyloid-beta pathology. Brain 139: 1265-1281. https://doi.org/10.1093/brain/aww016

32 Terry RD, Masliah E, Salmon DP, Butters N, DeTeresa R, Hill R, Hansen LA, Katzman R (1991) Physical basis of cognitive alterations in Alzheimer's disease: synapse loss is the major correlate of cognitive impairment. Ann Neurol 30: 572-580. https://doi.org/10.1002/ana.410300410

33 Ye L, Hamaguchi T, Fritschi SK, Eisele YS, Obermuller U, Jucker M, Walker LC (2015) Progression of seed-induced Abeta deposition within the limbic connectome. Brain Pathol 25: 743-752. https://doi.org/10.1111/bpa.12252

FIGURES

Figure 1

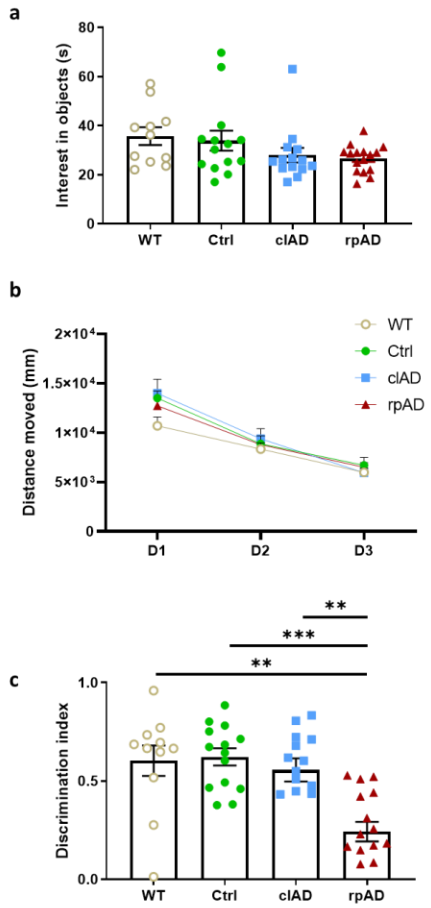

Figure 1. Object recognition deficits in the rpAD-inoculated mice. Object recognition performances were evaluated at 8 mpi in a V-maze. WT mice and $APP_{swe}/PS1_{de9}$ mice inoculated with Ctrl, clAD or rpAD brains had comparable exploratory activity, as suggested by the time spent on exploring the objects (a) ($p>0.05$; Kruskal-Wallis with Dunn's multiple comparisons) and the distance moved throughout the 3-day test (b) (for the days: $F_{(1.75, 89.47)} = 91.97$, $p<0.0001$; for the groups: $F_{(3, 51)} = 0.89$, $p=0.45$; two-way repeated measures ANOVA with the Geisser-Greenhouse correction and Dunnett's multiple comparisons). During the novel object recognition evaluation, rpAD mice spent less time exploring the novel object, as suggested by a lower discrimination index, compared to WT and $APP_{swe}/PS1_{dE9}$ clAD or Ctrl-inoculated mice (c) (respectively, $p=0.0018$, 0.0007 and 0.0082; Kruskal-Wallis with Dunn's multiple comparisons). **$p<0.01$; ***$p<0.001$. Data are shown as mean ± s.e.m.

Figure 2

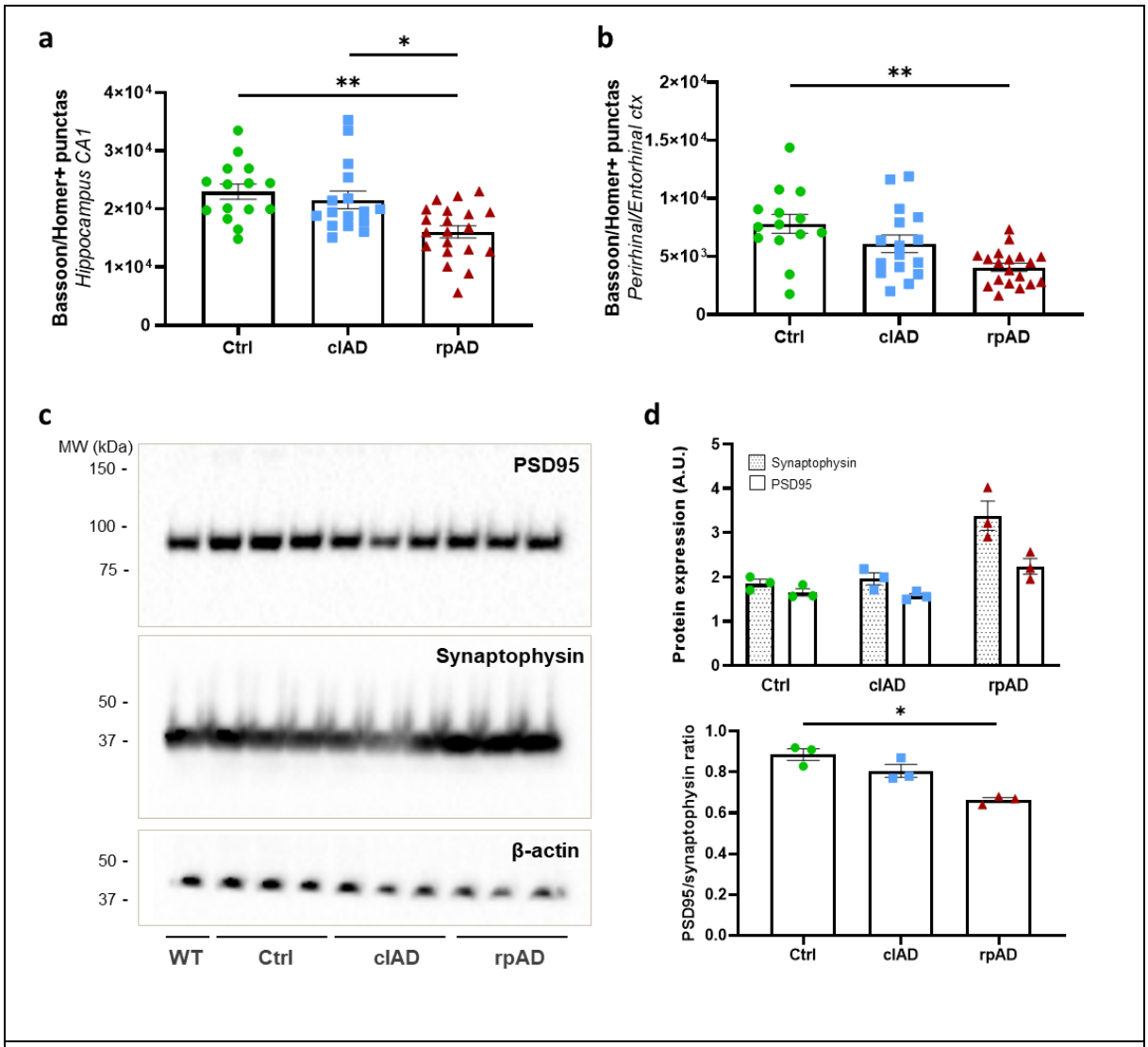

Figure 2. Synaptotoxicity is associated with rpAD brain extract inoculation. Quantification of Bassoon and Homer colocalization revealed a decrease in synaptic density in rpAD mice in the CA1 (a) and perirhinal/entorhinal cortex (b), compared to Ctrl and/or clAD-inoculated mice at 8 mpi. Western blots of hippocampal extracts (c) showing a decrease in the PSD95/synaptophysin ratio in the rpAD group compared to the Ctrl group (d). Kruskal-Wallis with Dunn's multiple comparisons. *p<0.05; **p<0.01. Data are shown as mean ± s.e.m.

Figure 3

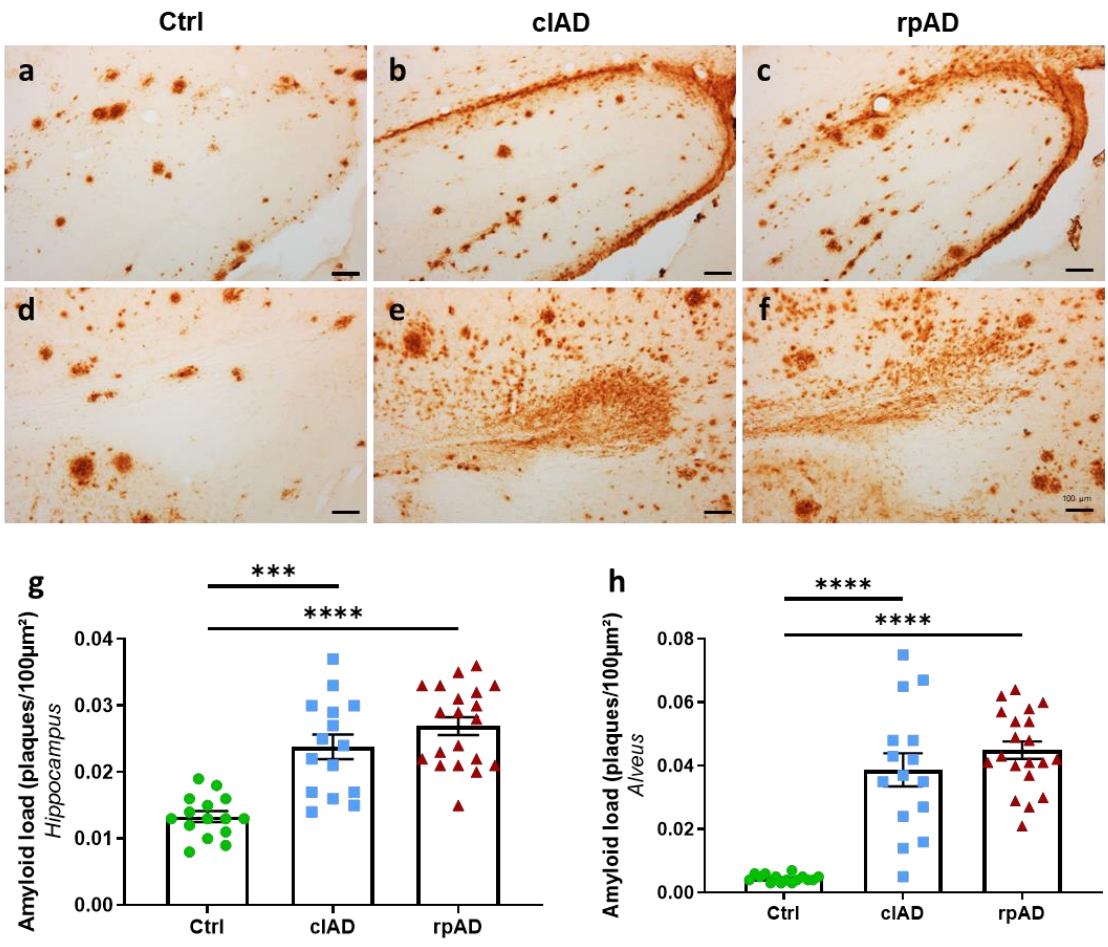

Figure 3. AD brain inoculation accelerates amyloidosis in $APP_{swe}/PS1_{de9}$ mice close to the injection site. (a-f) Representative images of 4G8 immunolabeling showing amyloid pathology in the hippocampus (a-c) and alveus (d-f) of $APP_{swe}/PS1_{dE9}$ mice eight months after human brain inoculation. (g-h) Quantification of amyloid load (4G8-positive amyloid plaques per 100 µm²) revealed that AD (clAD and rpAD) brain inoculation accelerates amyloid deposition in the hippocampus (g) and alveus (h). Kruskal-Wallis with Dunn's multiple comparisons. ***p<0.001; ****p<0.0001. Data are shown as mean ± s.e.m. Scale bars = 100 µm.

Figure 4

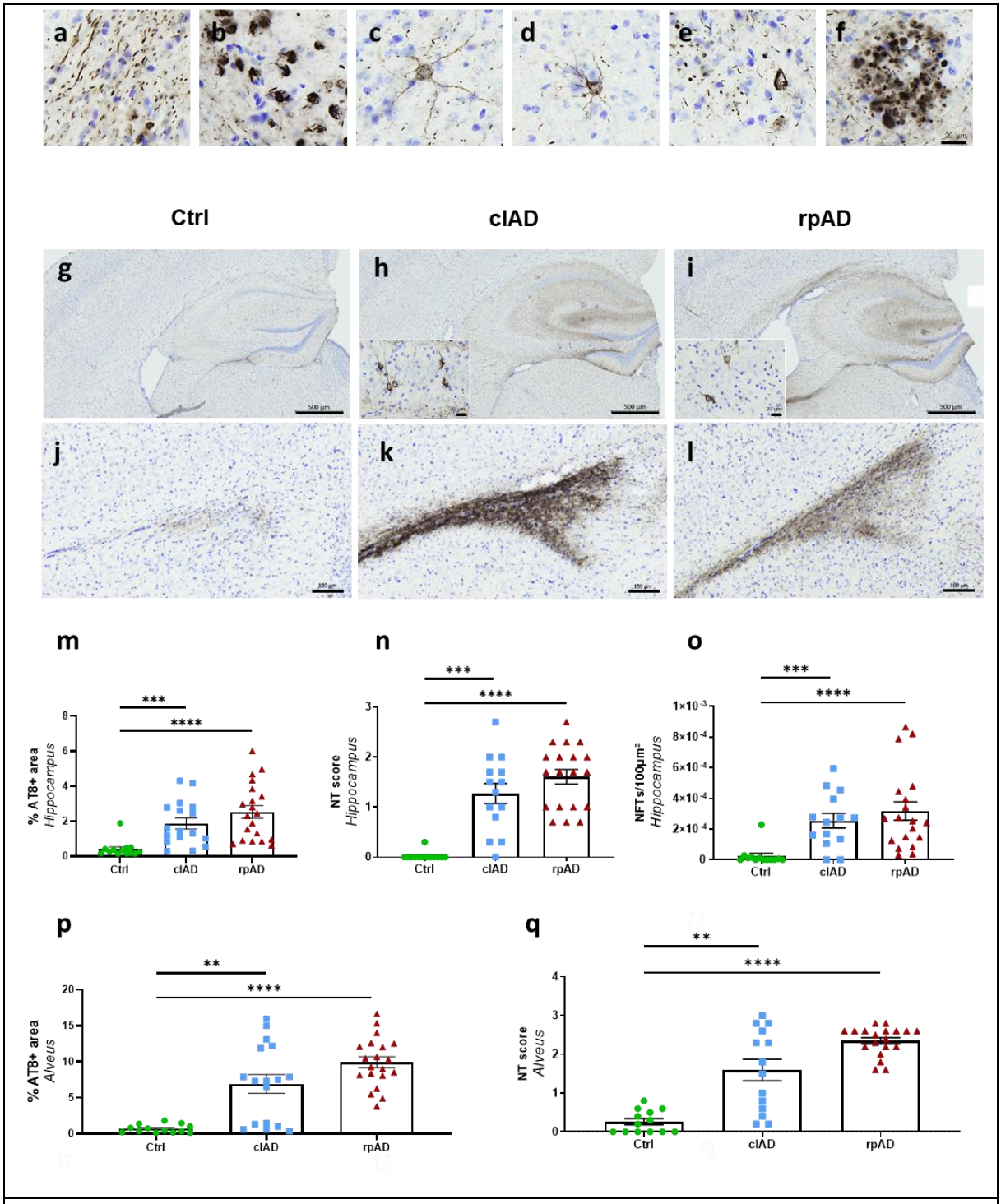

Figure 4. AD brain inoculation induces tau pathology in $APP_{swe}/PS1_{de9}$ mice close to the injection site at 8 mpi. AT8 immunolabeling revealed tau lesions in the forms of neuropil threads (a), neurofibrillary tangles (b-e) and neuritic plaques (f). (g-l) Representative images of AT8 immunolabeling showing tau pathology induction in the hippocampus (g-i) and alveus (j-l) of $APP_{swe}/PS1_{de9}$ mice eight months after human brain inoculation. Quantification of overall AT8-labelled phospho-tau (percentage of AT8-positive area), NTs scoring and NFTs accumulation (AT8-

positive NFTs per 100 µm² of area) in the hippocampus (m-o) and/or alveus (p-q) showed an increase in tau pathology following clAD and rpAD brain inoculation compared to Ctrl brain. *p<0.05; **p<0.01; ***p<0.001; ****p<0.0001 (Kruskal-Wallis with Dunn's multiple comparisons test). Data are shown as mean ± s.e.m. Scale bars = 20 µm (a-f and inserts), 500 µm (g-i) and 100 µm (j-l).

Figure 5

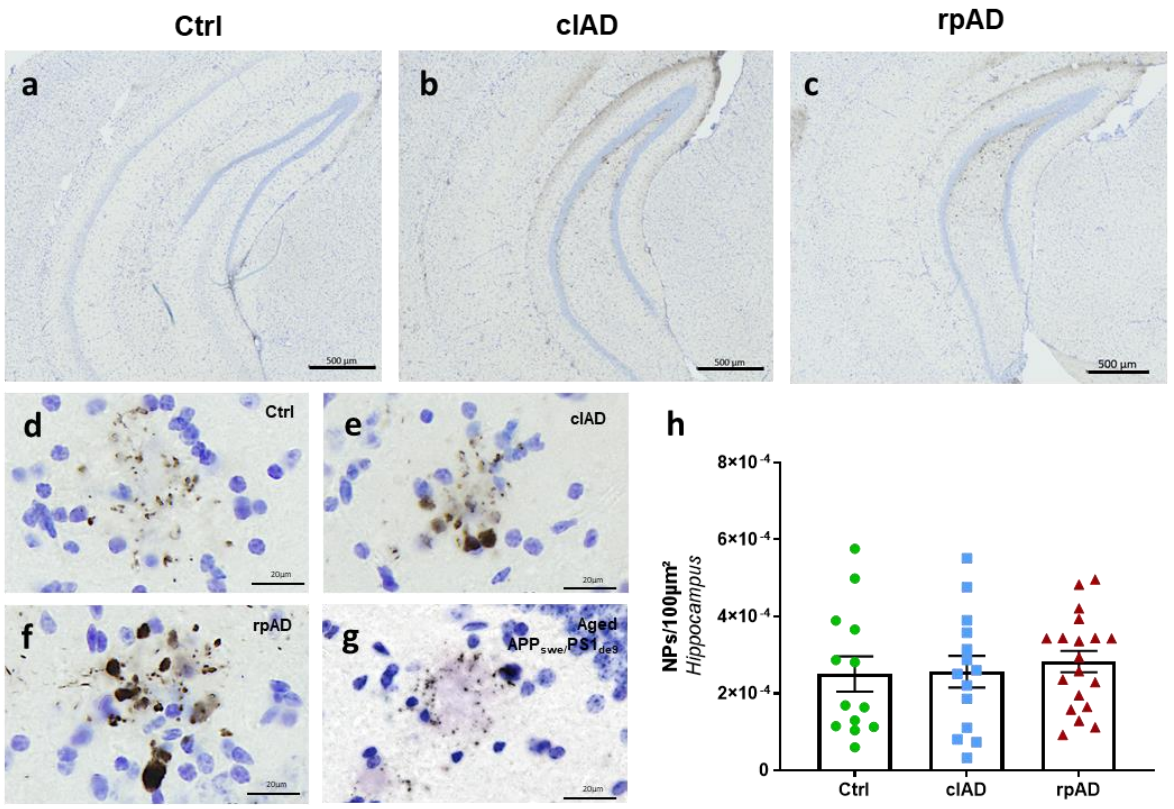

Figure 5. Neuritic plaques in $APP_{swe}/PS1_{de9}$ mice. (A-C) Representative images of AT8-positive neuritic plaques in Ctrl- (a, d) and AD-inoculated (b and e for clAD, c and f for rpAD) mice. Quantification revealed similar NP counts (NPs per 100 µm² of area) in all groups (h). AT8 immunolabeling of non-inoculated aged $APP_{swe/}PS1_{de9}$ mice (24 months old) also revealed NPs (g). Data are shown as mean ± s.e.m. Scale bars = 500 µm (a-c) and 20 µm (d-g).

Figure 6

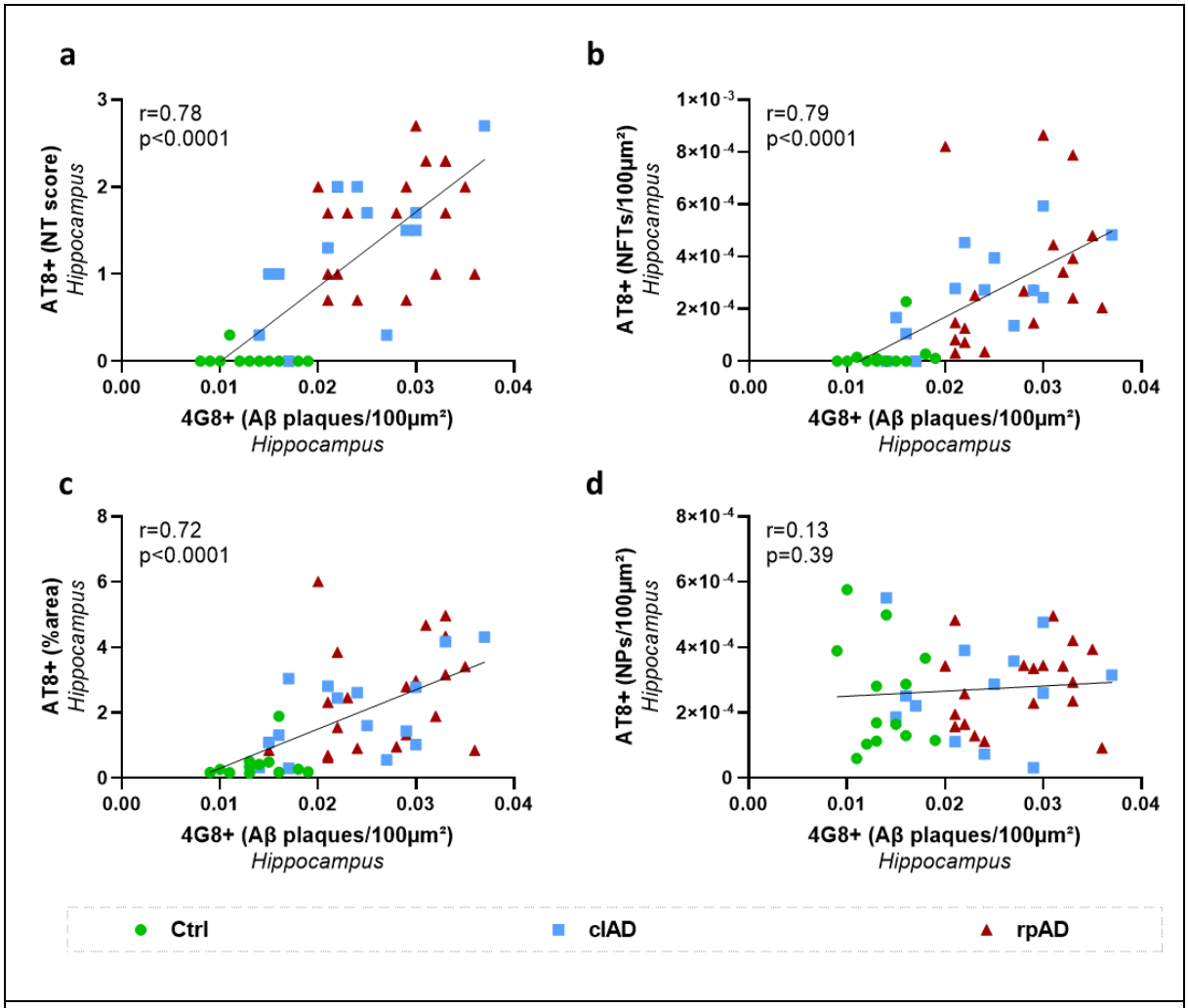

Figure 6. Amyloid and tau lesions were correlated in the hippocampus of inoculated mice. Amyloid loads were correlated to NT scores (a) ($r_{spearman\text{-}hip}$=0.78, p<0.0001), NFTs (b) ($r_{spearman\text{-}hip}$=0.79, p<0.0001) and to the global tau pathology (c) ($r_{spearman\text{-}hip}$=0.72, p<0.0001) but not to NPs (d) ($r_{spearman\text{-}hip}$=0.13, p=0.39), in the hippocampus of Ctrl-, clAD- and rpAD-inoculated mice.

Figure 7

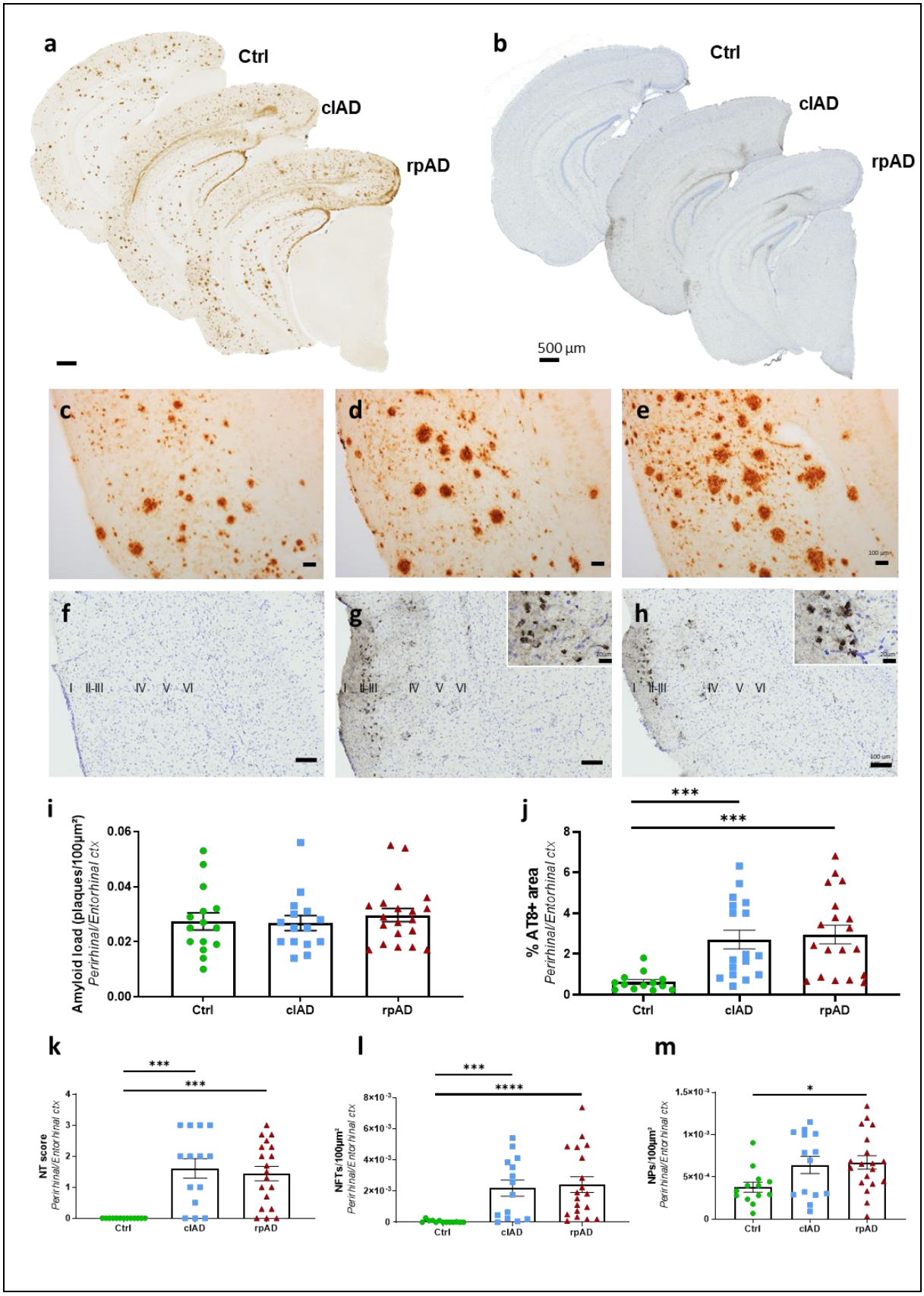
a
Ctrl
cIAD
rpAD
b
Ctrl
cIAD
rpAD
500 µm
c
d
e
f
g
h
I II-III IV V VI
i
Amyloid load (plaques/100µm²)
Perirhinal/Entorhinal ctx
0.06
0.04
0.02
0.00
Ctrl
cIAD
rpAD
j
***
***
% AT8+ area
Perirhinal/Entorhinal ctx
8
6
4
2
0
Ctrl
cIAD
rpAD
k
***
***
NT score
Perirhinal/Entorhinal ctx
4
3
2
1
0
Ctrl
cIAD
rpAD
l
***
****
NFTs/100µm²
Perirhinal/Entorhinal ctx
8x10⁻³
6x10⁻³
4x10⁻³
2x10⁻³
0
Ctrl
cIAD
rpAD
m
*
NPs/100µm²
Perirhinal/Entorhinal ctx
1.5x10⁻³
1x10⁻³
5x10⁻⁴
0
Ctrl
cIAD
rpAD

Figure 7. Tau but not amyloid spreading following AD brain inoculation in $APP_{swe}/PS1_{de9}$ mice. Representative images of the 4G8 immunolabeling showing amyloid pathology (a) and the AT8 immunolabeling showing tau pathology (b) in AD-inoculated $APP_{swe}/PS1_{de9}$ mice. Magnified views of amyloid (c-e) and tau (f-h) lesions in the perirhinal/entorhinal cortex. Quantification of amyloid load (i), overall AT8-positive tau lesions (j), NTs (k), NFTs (l) and NPs (m) in the perirhinal/entorhinal cortex. Kruskal-Wallis with Dunn's multiple comparisons test. ***$p<0.001$; ****$p<0.0001$. Data are shown as mean ± s.e.m. Scale bars = 500 µm (a-b), 100 µm (c-h) and 20 µm in inserts.

Figure 8

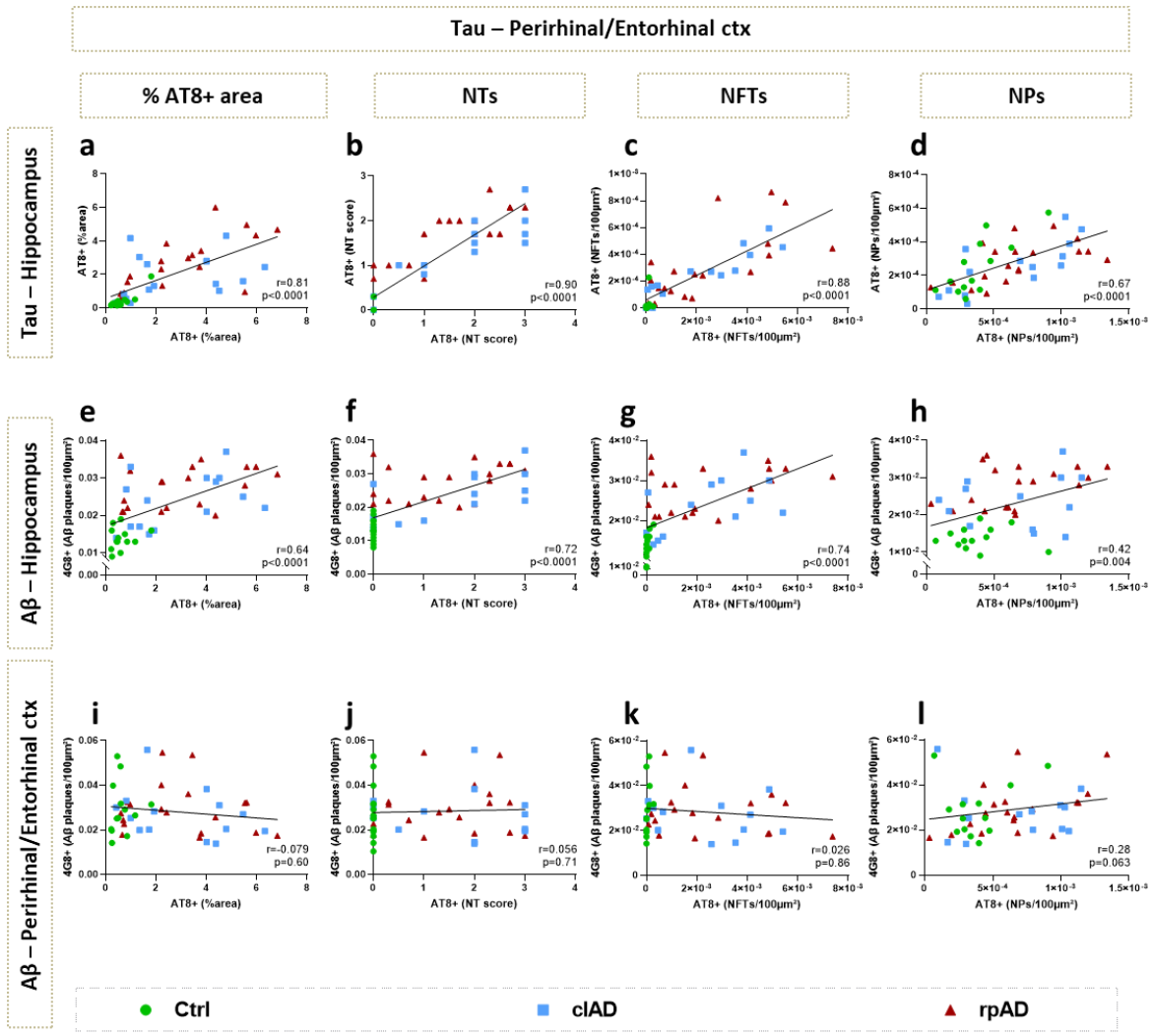

Figure 8. Correlations between tau in the perirhinal/entorhinal cortex and amyloid or tau lesions in the hippocampus and perirhinal/entorhinal cortex. All of tau pathological markers in the perirhinal/entorhinal cortex were strongly correlated to tau markers in the hippocampus (a-d) and amyloid load in the hippocampus (e-h). Unexpectedly, none of tau perirhinal/entorhinal lesions were correlated to amyloid load in this same region (i-l). Spearman's correlations with significance level set at $p<0.05$.

Figure 9

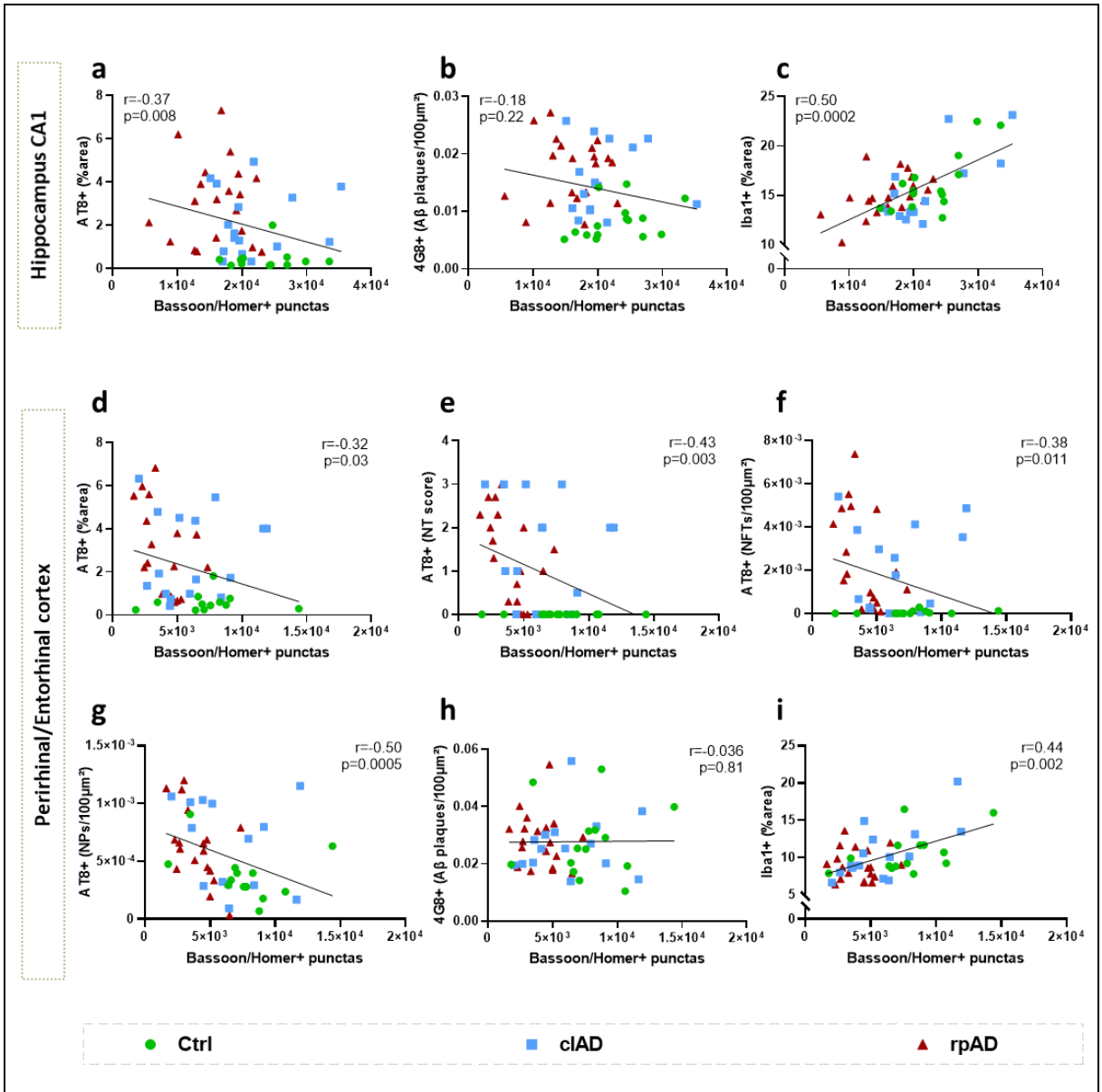

Figure 9. Correlations between synaptic density and tau lesions, Aβ plaque load or microglial activity. Synaptic density (Bassoon/Homer+ puncta) was negatively correlated to tau pathology both in the hippocampus (a) and the perirhinal/entorhinal cortex (d-h), but not to amyloid pathology (b, i). Interestingly, synaptic density was positively correlated with microglial Iba1 labelling in the hippocampus (c) as well as in the perirhinal/entorhinal cortex (j). Spearman's correlations with significance level at $p<0.05$.

Figure 10

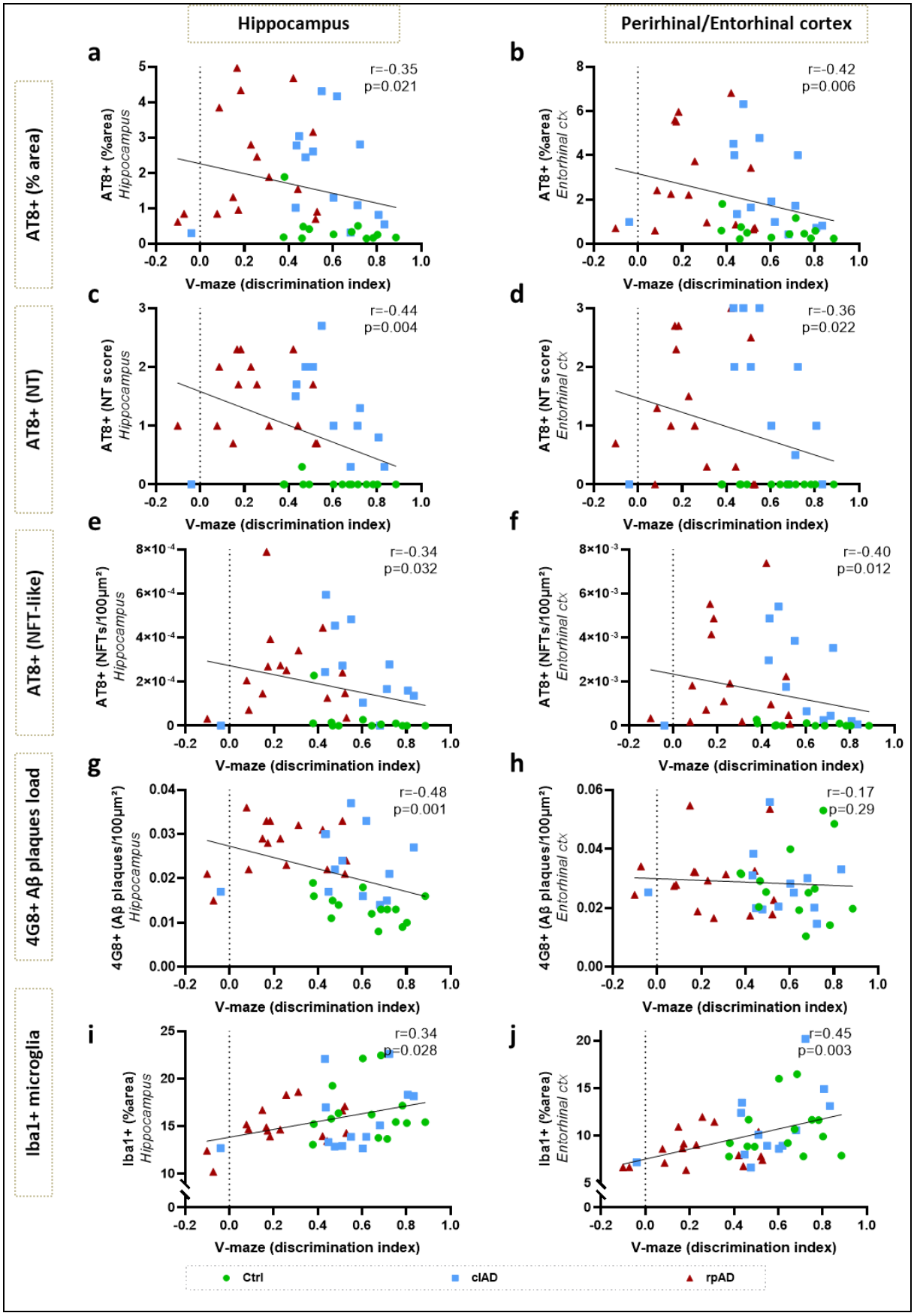
Hippocampus
Perirhinal/Entorhinal cortex
AT8+ (% area)
AT8+ (NT)
AT8+ (NFT-like)
4G8+ Aβ plaques load
Iba1+ microglia
a
AT8+ (%area) Hippocampus
r=-0.35
p=0.021
b
AT8+ (%area) Entorhinal ctx
r=-0.42
p=0.006
c
AT8+ (NT score) Hippocampus
r=-0.44
p=0.004
d
AT8+ (NT score) Entorhinal ctx
r=-0.36
p=0.022
e
AT8+ (NFTs/100µm²) Hippocampus
r=-0.34
p=0.032
f
AT8+ (NFTs/100µm²) Entorhinal ctx
r=-0.40
p=0.012
g
4G8+ (Aβ plaques/100µm²) Hippocampus
r=-0.48
p=0.001
h
4G8+ (Aβ plaques/100µm²) Entorhinal ctx
r=-0.17
p=0.29
i
Iba1+ (%area) Hippocampus
r=0.34
p=0.028
j
Iba1+ (%area) Entorhinal ctx
r=0.45
p=0.003
V-maze (discrimination index)
Ctrl
cIAD
rpAD

Figure 10. Correlations between V-maze cognitive scores and tau lesions, Aβ plaque load or microglial activation. V-maze cognitive scores (discrimination index) were negatively correlated to tau pathology both in the hippocampus and the perirhinal/entorhinal cortex (a-f). Cognitive scores were correlated to amyloid pathology in the hippocampus (g) but not in the perirhinal/entorhinal cortex (h). Microglial Iba1-positive staining was positively correlated to cognitive scores in both regions (i-j). Spearman's correlations with significance level at $p<0.05$.

Figure 11

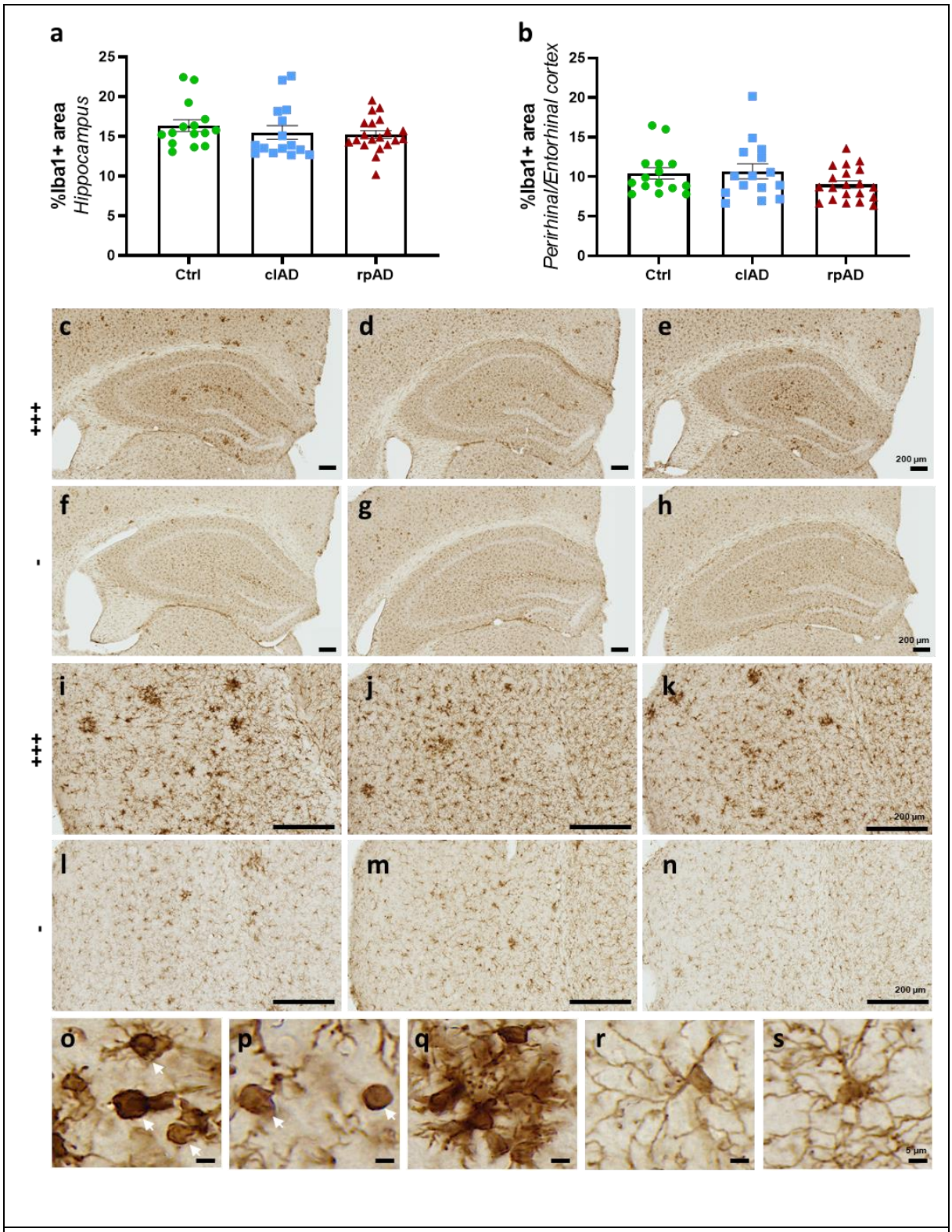

Figure 11. Heterogeneous microglial activation in AD- and Ctrl-inoculated $APP_{swe}/PS1_{de9}$ mice. Overall Iba1-positive staining quantification revealed similar levels of Iba1 in the hippocampus (a) and perirhinal/entorhinal cortex (b) of all three groups (Kruskal-Wallis test). Within each group, animals with high and low Iba1 staining were identified. Representative images of animals with

higher Iba1 levels showing abundant activated microglia clustering around Aβ plaques in the hippocampus (c-e) and perirhinal/entorhinal cortex (i-k). Animals with lower Iba1 levels displayed more cells with a highly ramified profile, consistent with a non-activated phenotype (f-h, l-n). Activated microglia were characterized by beading with spheroidal swellings of the processes and enlarged cell body with dystrophic ramifications (o-p, arrows). These activated cells formed microglial clusters surrounding Aβ plaques (q). Highly ramified microglia in an animal with low Iba1 labelling close to amyloid plaques (r) or far from plaques (s). Data are shown as mean ± s.e.m. Scale bars = 200 µm (c-n) and 5 µm (o-s).

SUPPLEMENTARY MATERIALS

SUPPLEMENTARY TABLE

Supplementary Table 1

Patient				Neuropathology							
ID	Age	Gender	Disease progression (months)	Post mortem delay (hours)	Braak stage	Thal stage	CAA	α-synuclein	TDP43	Hippocampal sclerosis	PrPSc
Ctrl1	66	M	-	26	II	0	0	0	0	0	0
Ctrl2	76	M	-	?	II	0	0	0	0	0	0
clAD1	79	F	78	48.6	V	5	Type2 +	0	0	0	0
clAD2	87	F	72	29	V-VI	4	Type1 +++	0	0	0	0
clAD3	89	F	96	30.6	V	5	Type1	0	0	0	0
clAD4	71	M	66	54	VI	4	Type2 +	Amygdala	0	0	0
rpAD1	84	F	6	79	IV	4	Type2	0	0	0	0
rpAD2	81	F	36	?	V	5	Type1	0	0	0	0
rpAD3	81	F	36	26	VI	4	0	0	0	0	0
rpAD4	86	F	36	20.5	V	4	Type2	0	0	0	0

Supplementary Table 1. Patient characteristics. Age-matched classical and rapidly evolving AD patients were selected based on disease duration (over or under 36 months) and neuropathological evaluation, including similar Braak and Thal stages. Brains were negative for α-synuclein, TDP43, hippocampal sclerosis and pathological prion PrPSc. Two non-AD control individuals were also included in this study.

SUPPLEMENTARY FIGURES

Supplementary Figure 1

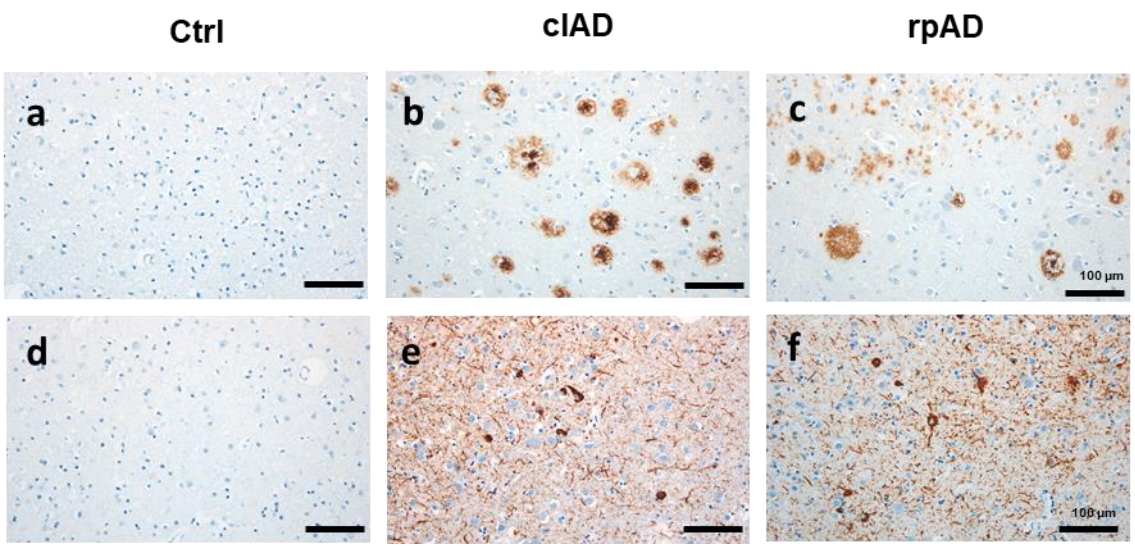

Supplementary Figure 1. Amyloid and tau pathological evaluations in human brain samples. Representative images of Ctrl, clAD and rpAD brain sample stainings for amyloid (a-c) and tau (d-f) pathologies. Scale bars = 100 µm.

Supplementary Figure 2

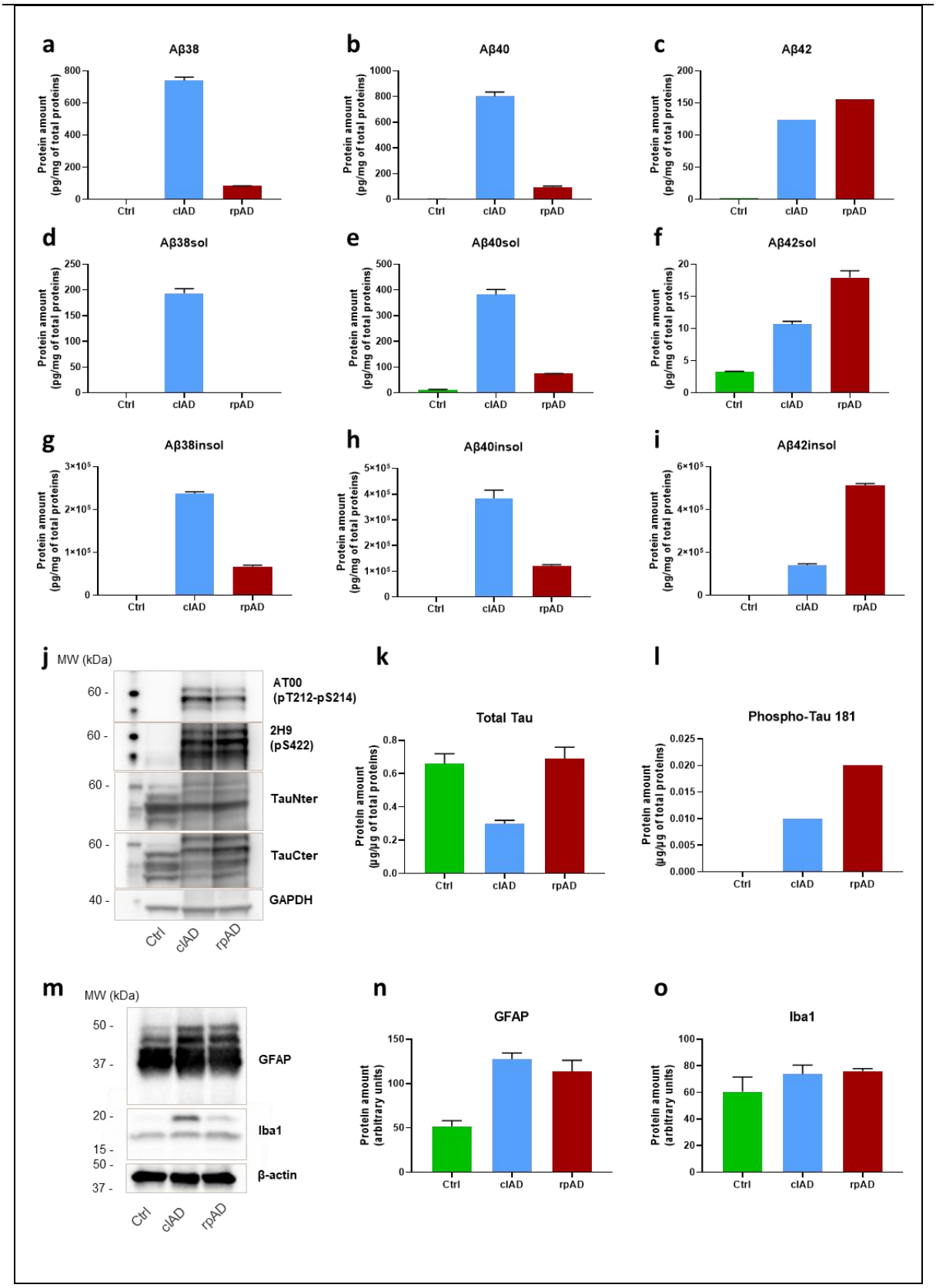

Supplementary Figure 2. Biological characteristics of brain homogenates inoculated to animals. Three brain homogenates were prepared from the 2 Ctrl (Ctrl homogenate), 4 clAD (clAD homogenate) and 4 rpAD cases (rpAD homogenate). All quantifications of the inoculated brain homogenates (Ctrl, clAD or rpAD) were performed in duplicate and data are shown as mean ± s.d of the replicates. (a-i) Quantifications of total, soluble and insoluble $A\beta_{38}$, $A\beta_{40}$ and $A\beta_{42}$ of the inoculated brain extracts (MSD technology). Both AD inocula had more Aβ proteins compared to the Ctrl one. The clAD inoculum showed more $A\beta_{38}$ and $A\beta_{40}$ but less $A\beta_{42}$ than the rpAD one. (j-l) Tau profile evaluation revealed a pathological hyperphosphorylated tau triplet at 60, 64 and 69 kDa observed in AD and a typical shift in the molecular weight of the Alzheimer Tau-Cter triplet in western blots (j). Total tau (k) and pathological phospho-tau 181 levels (l) were assessed using ELISA quantification. (m-o) Neuroinflammatory profile evaluation by western blots revealed higher astrocytic presence (GFAP-positive) in clAD and rpAD inocula compared to the Ctrl extract (M-N). Microglial (Iba1-positive) levels were similar in the Ctrl, clAD and rpAD groups (m, o).

Supplementary Figure 3

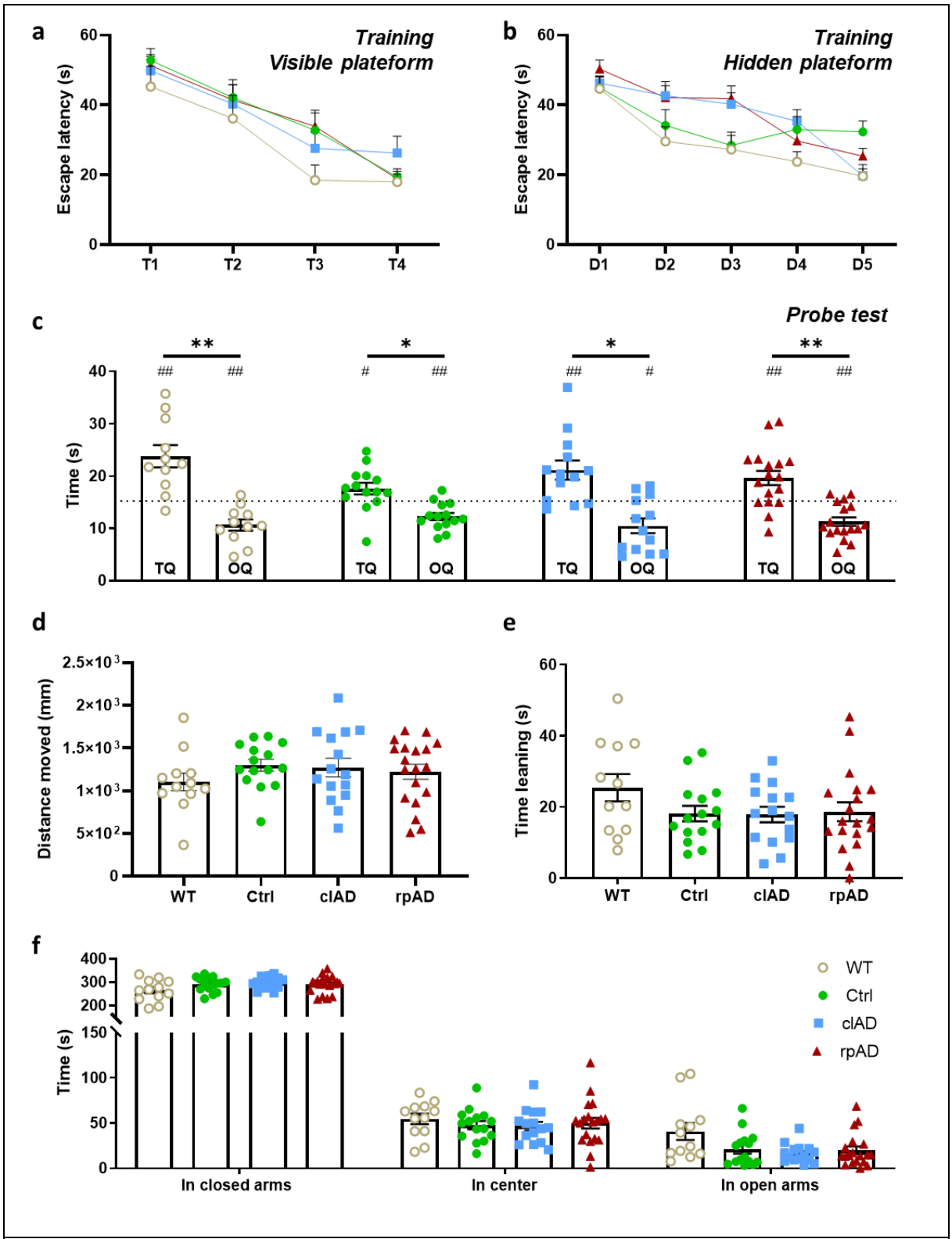

Supplementary Figure 3. Inoculated mice showed similar spatial memory performances and anxiety levels at 8 mpi. (a-c) Spatial memory was assessed using the Morris water maze test. During the visible plateform phase (a), escape latencies steadily decreased across the four trials ($F_{(2.649, 135.1)}$ = 36.67, p<0.0001; two-way repeated measures ANOVA with the Geisser-Greenhouse correction

and Dunnett's multiple comparisons). No difference was observed between the groups ($F_{(3, 51)}$=1.87, p=0.15; two-way repeated measures ANOVA with the Geisser-Greenhouse correction and Dunnett's multiple comparisons). For the hidden platform training phase (b), escape latencies were averaged across three trials per day and slowly decreased across the trials and days suggesting that mice had succesfully learnt the platform position ($F_{(3.575, 182.3)}$ = 36.09, p<0.0001; two-way repeated measures ANOVA with the Geisser-Greenhouse correction and Dunnett's multiple comparisons). No difference was observed between the groups suggesting that Ctrl, clAD and rpAD brain inoculations do not differentially impact spatial learning abilities in $APP_{swe}/PS1_{dE9}$ mice after an eight-month incubation period ($F_{(2, 41)}$=0.85, p=0.88; two-way repeated measures ANOVA with the Geisser-Greenhouse correction and Dunnett's multiple comparisons). During the probe test (c), the time spent in the target quadrant (TQ) was significantly higher than the time spent in the opposite one (OQ) (*p<0.05; two-way repeated measures ANOVA with the Geisser-Greenhouse correction and Dunnett's multiple comparisons). Moreover, the time spent both in the TQ and OQ was significantly different from 15 seconds, which corresponds to 25% of the trial duration (# p<0.05; one-sample Wilcoxon's signed-rank test). Spatial memory retention was evaluated after 72 hours. All groups performed as well as the WT group by spending more time in the target quadrant than in the opposite one, suggesting that memory is not impaired in $APP_{swe}/PS1_{dE9}$ Ctrl or AD-inoculated mice (for the groups: $F_{(3, 51)}$ = 0.83, p>0.05; for TQ versus OQ: p=0.0028, 0.0217, 0.0117 and 0.0013, respectively for Wt, Ctrl, clAD and rpAD groups; two-way ANOVA with the Geisser-Greenhouse correction and Dunnett's multiple comparisons). (d-f) Anxiety levels were assessed using the elevated plus maze. Comparable travelled distance (d), time spent leaning over the maze (e) and time spent in the different areas of the maze (open/closed arms and center of the maze) (f) were reported between the groups (p>0.05; Kruskal-Wallis' test). Data are shown as mean ± s.e.m.

Supplementary Figure 4

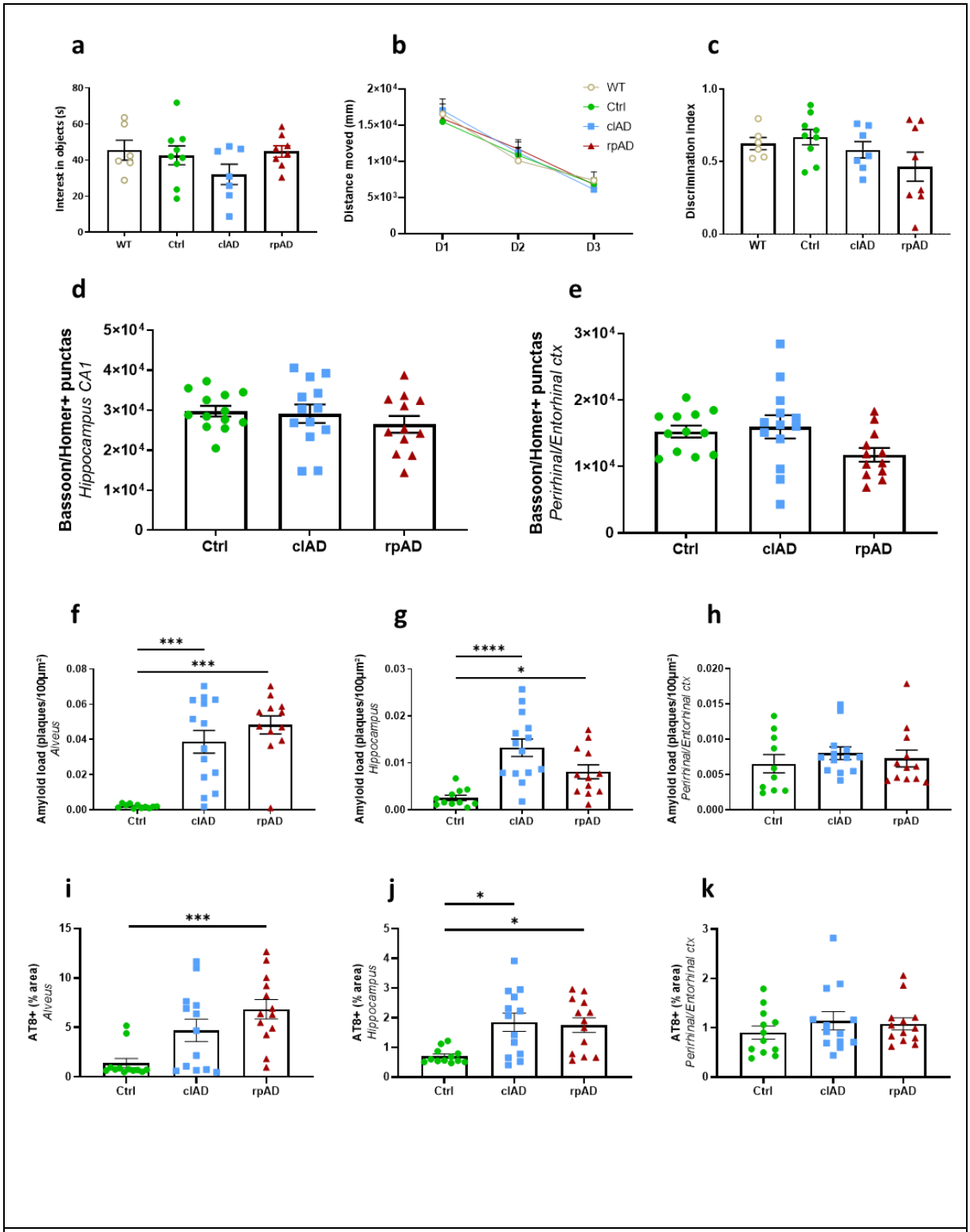

Supplementary Figure 4. Cognitive performance, synaptic density, amyloid and tau loads evaluations at 4 mpi. (a-c) Object recognition performances were evaluated at 4 mpi using a V-maze test. WT mice and $APP_{swe}/PS1_{de9}$ mice inoculated with Ctrl, clAD or rpAD brains had comparable exploratory activity, as suggested by the time spent on exploring the objects (a) ($p>0.05$; Kruskal-

Wallis with Dunn's multiple comparisons) and the distance moved throughout the 3-day test (b) (for the days: $F_{(1.89, 49.15)} = 152.6$, $p<0.0001$; for the groups: $F_{(3, 26)} = 0.041$, $p=0.99$; two-way repeated measures ANOVA with the Geisser-Greenhouse correction and Dunnett's multiple comparisons). No difference in the novel object recognition test was reported between the groups, as similar discrimination indexes were observed (c) ($p>0.05$; Kruskal-Wallis with Dunn's multiple comparisons). (d-e) Quantification of Bassoon and Homer colocalization at 4 mpi did not show any differences in the CA1 (d) and in the perirhinal/entorhinal cortex (e) between the groups ($p>0.05$; Kruskal-Wallis with Dunn's multiple comparisons). (f-h) Amyloid load quantification at 4 mpi revealed that AD (clAD and rpAD) brain inoculation accelerates amyloid deposition in the alveus (f) and hippocampus (g), but not the perirhinal/entorhinal cortex (h) (respectively for clAD and rpAD mice, in the alveus $p= 0.0008$ and 0.0003, in the hippocampus $p<0.0001$ and $p=0.041$, in the perirhinal/entorhinal cortex $p>0.05$; Kruskal-Wallis with Dunn's multiple comparisons). (i-k) AT8-positive tau overall quantification at 4 mpi revealed that AD (clAD and rpAD) brain inoculation induces tau lesions in the alveus (i) and hippocampus (j), but not the perirhinal/entorhinal cortex (k) (respectively for clAD and rpAD mice, in the alveus $p= 0.080$ and 0.0006, in the hippocampus $p= 0.016$ and 0.011, in the perirhinal/entorhinal cortex $p>0.05$; Kruskal-Wallis with Dunn's multiple comparisons). *$p<0.05$; ***$p<0.001$; ****$p<0.0001$. Data are shown as mean ± s.e.m.

Supplementary Figure 5

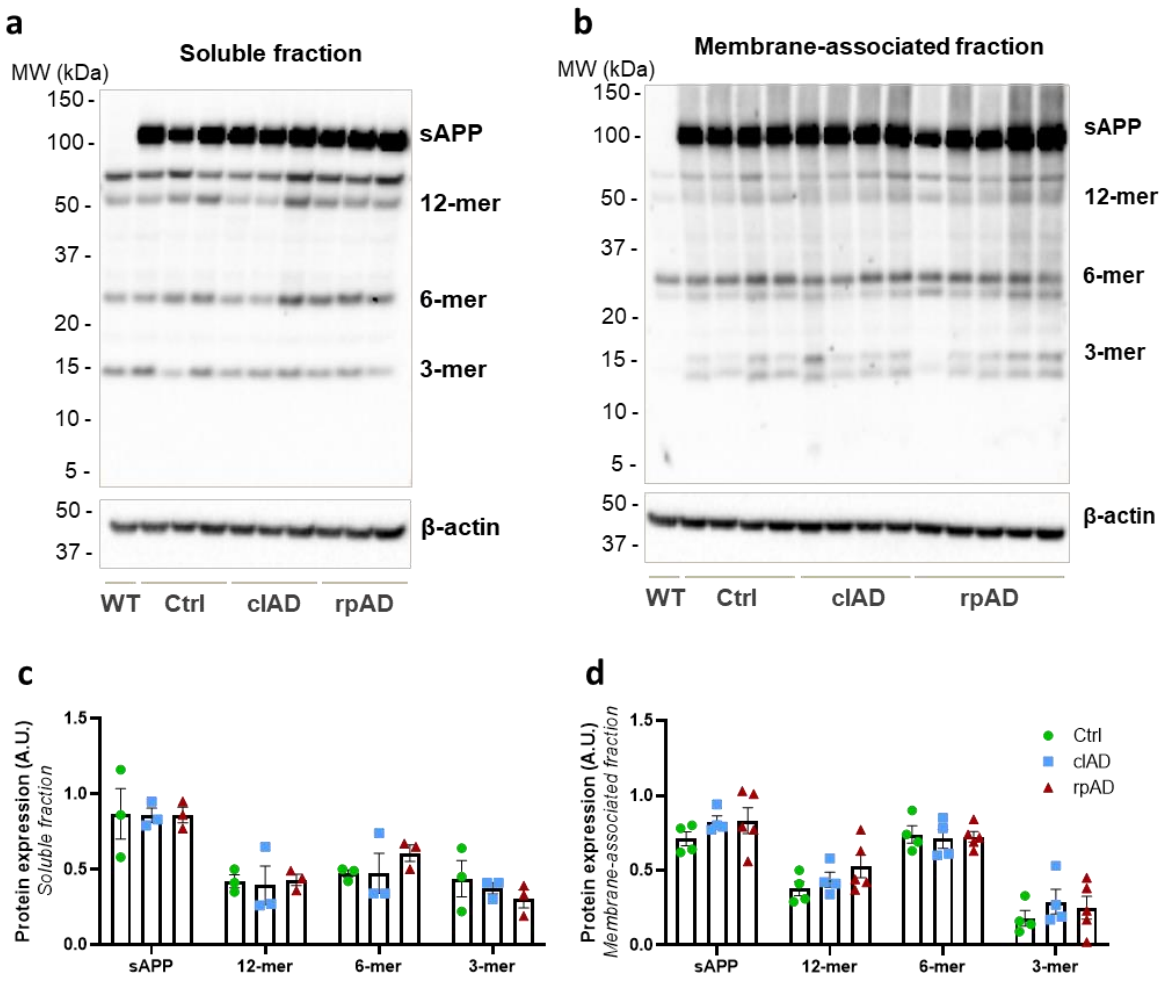

Supplementary Figure 5. Similar amounts of soluble and membrane-associated amyloid are found in AD- and Ctrl-inoculated $APP_{swe}/PS1_{de9}$ mice. Western blots of hippocampal extracts showing that soluble (a) and membrane-associated (b) Aβ loads are similar in AD- and Ctrl-inoculated $APP_{swe}/PS1_{de9}$ mice (c-d). Protein expression was normalized by β-actin level. $p>0.05$; Kruskal-Wallis' test. Data are shown as mean ± s.e.m.

Supplementary Figure 6

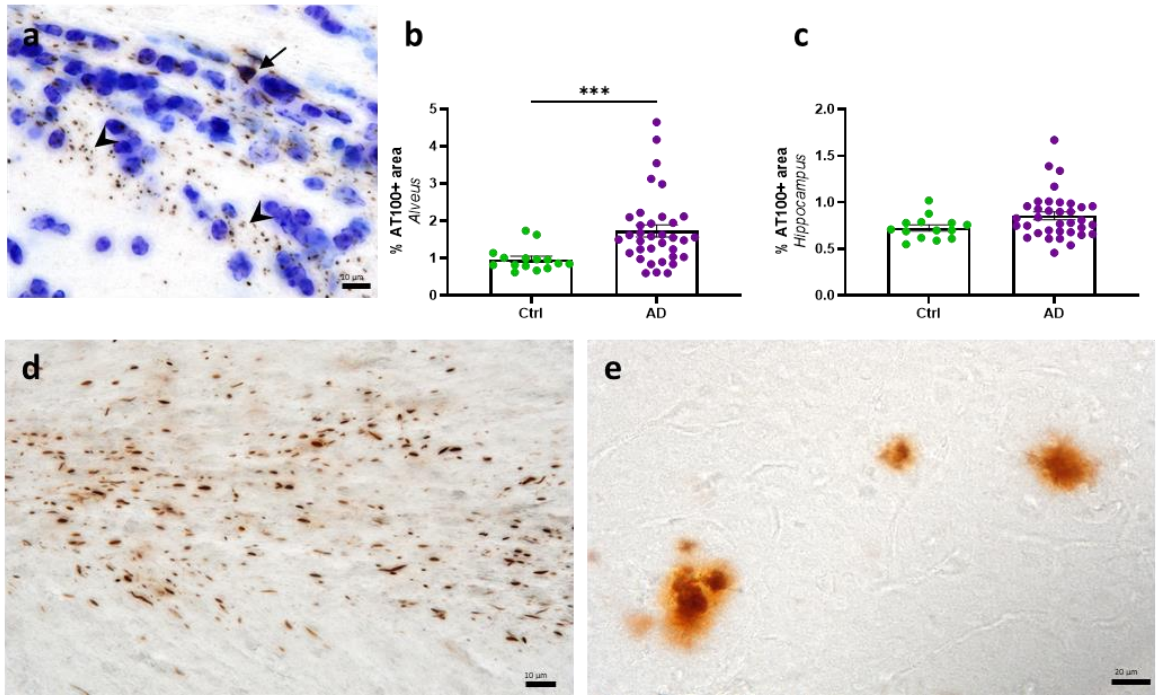

Supplementary Figure 6. AT100 and Gallyas-positive lesions next to the inoculation site of $APP_{swe}/PS1_{de9}$ mice 8 months after AD brain extracts injection. (a) AT100 staining revealed NTs (arrow heads) and NFTs (arrow). (b-c) Overall quantification of AT100 labelling showed increased labelling in the alveus (b) and a trend for increased labelling in the hippocampus (c) of AD inoculated mice (p=0.0007 and 0.092 respectively, Mann-Whitney test). Gallyas silver staining revealed neuropil threads (d) as well as amyloid plaques (e) in inoculated mice. Data are shown as mean ± s.e.m. Scale bars = 10 µm (a, d) and 20 µm (e).

Supplementary Figure 7

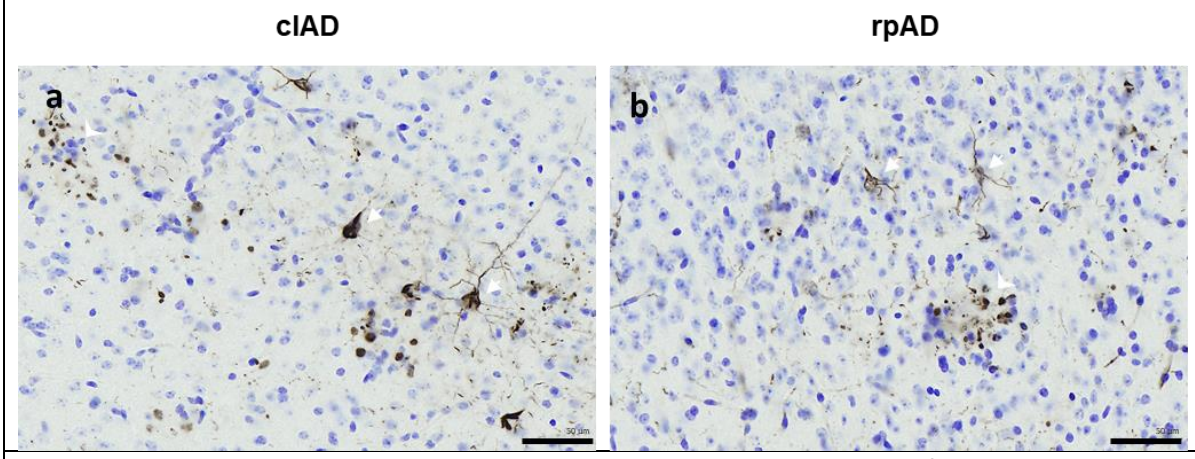

Supplementary Figure 7. AT8-positive lesions in the visual cortex of $APP_{swe}/PS1_{de9}$ mice 8 months after AD brain extract inoculation. AT8 staining revealed NFTs (arrows) surrounded by NTs, as well as NPs (arrow heads), in clAD (a) and rpAD (b) brain inoculation. Scale bars = 50 µm.

Supplementary Figure 8

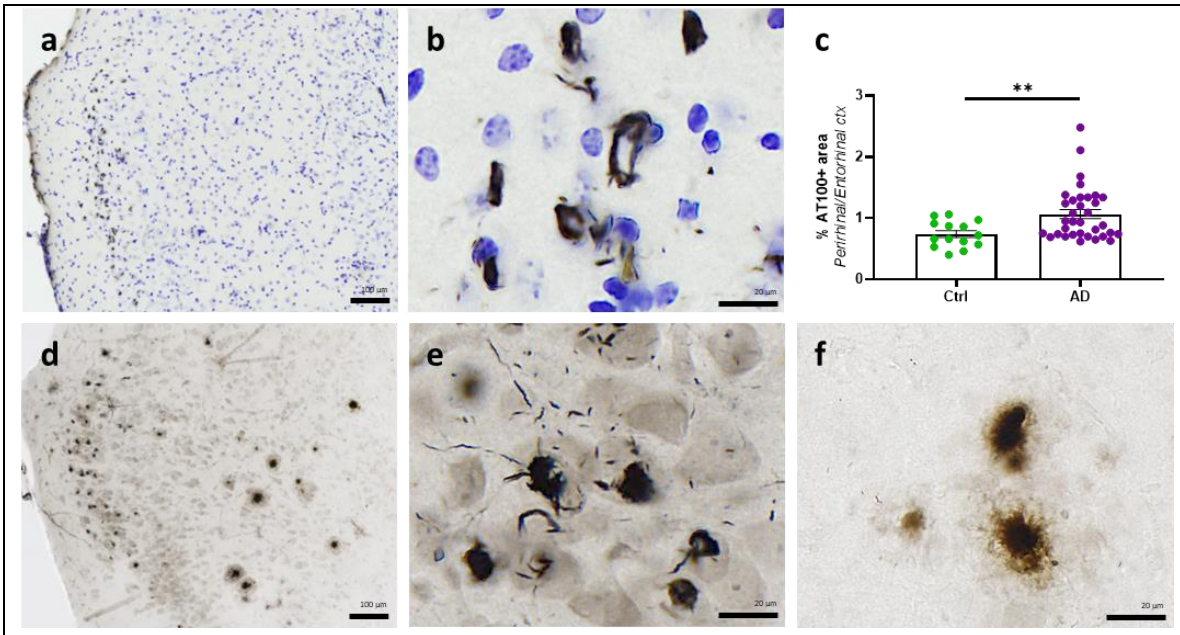

Supplementary Figure 8. AT100 and Gallyas positive lesions spreading to the perirhinal/entorhinal cortex of $APP_{swe}/PS1_{de9}$ mice 8 months after AD brain extract injection. (a-b) AT100 staining revealed NFTs in the perirhinal/entorhinal cortex. (c) Overall quantification of AT100 labelling showed increased labelling in the perirhinal/entorhinal cortex of AD inoculated mice compared to Ctrl-inoculated ones (p=0.005, Mann-Whitney test). (d-f) Gallyas silver staining revealed labelled neurons evoking NFTs (e) as well as amyloid plaques (f). Data are shown as mean ± s.e.m. Scale bars = 100 µm (a, d) and 20 µm (b, e, f).

Supplementary Figure 9

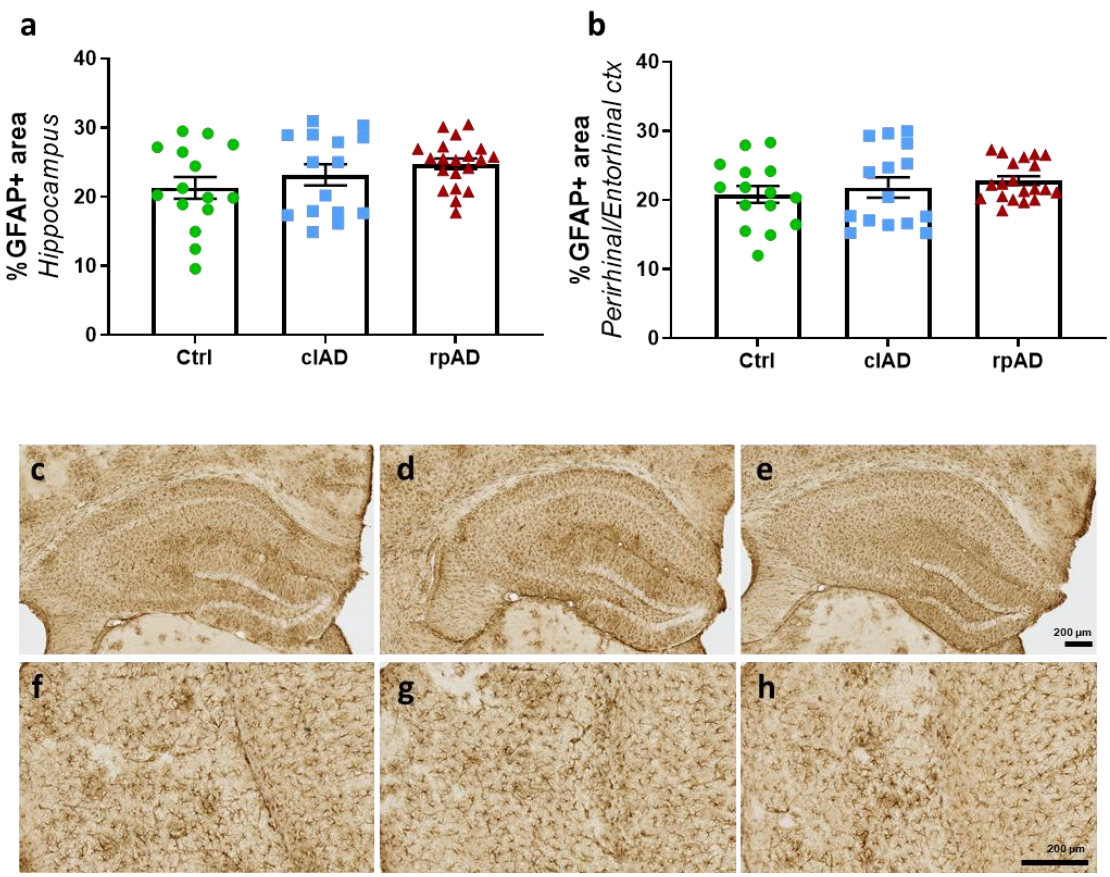

Supplementary Figure 9. Astrocytic coverage is similar in the hippocampus and perirhinal/entorhinal cortex of AD- and Ctrl-inoculated $APP_{swe}/PS1_{de9}$ mice at 8 mpi. GFAP staining revealed similar astrocytic loads in the hippocampus (a, c-e) and perirhinal/enthorhinal cortex (b, f-h) of Ctrl, clAD and rpAD-inoculated $APP_{swe}/PS1_{de9}$ mice at 8 mpi. Data are shown as mean ± s.e.m. Scale bars = 200 µm.

Supplementary Figure 10

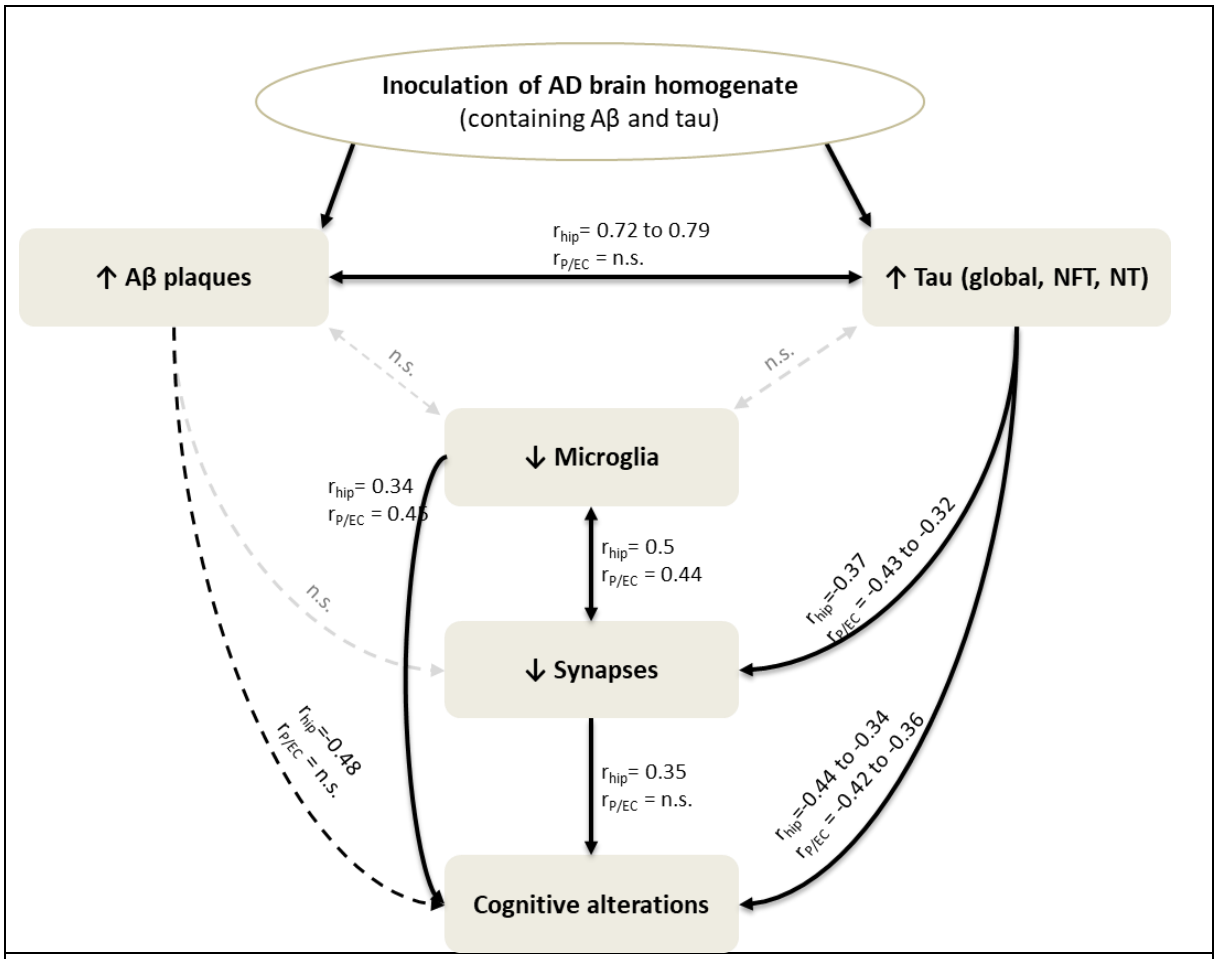

Supplementary Figure 10. Overview of the possible links between AD core lesions, synaptic and cognitive impairment. The inoculation of AD brain homogenates accelerates Aβ deposition and induces tau lesions in $APP_{swe}/PS1_{de9}$ mice. The severity of tau (but not amyloid) lesions and reduced microglial loads were associated with synaptic loss. Cognitive alterations were correlated with the severity of tau lesions and microglial reduction in both the hippocampus and the perirhinal/entorhinal cortex, and with amyloid loads in the hippocampus only. No direct link was found between microglia and tau or Aβ. Altogether, these data suggest that tau-seeded pathologies induced by AD brain inoculation and low microglial activity drive synaptic and cognitive deficits in Aβ plaque-bearing mice. Spearman correlations with a significance level set at 0.05.